NUCLEAR DATA AND MEASUREMENTS SERIES

ANL/NDM-141

Neutron Scattering and Models: Titanium

by

A.B. Smith

July 1997

ARGONNE NATIONAL LABORATORY,
ARGONNE, ILLINOIS 60439, U.S.A.

NUCLEAR DATA AND MEASUREMENTS SERIES

ANL/NDM-141

NEUTRON SCATTERING AND MODELS:- TITANIUM

A. B. Smith
July, 1997

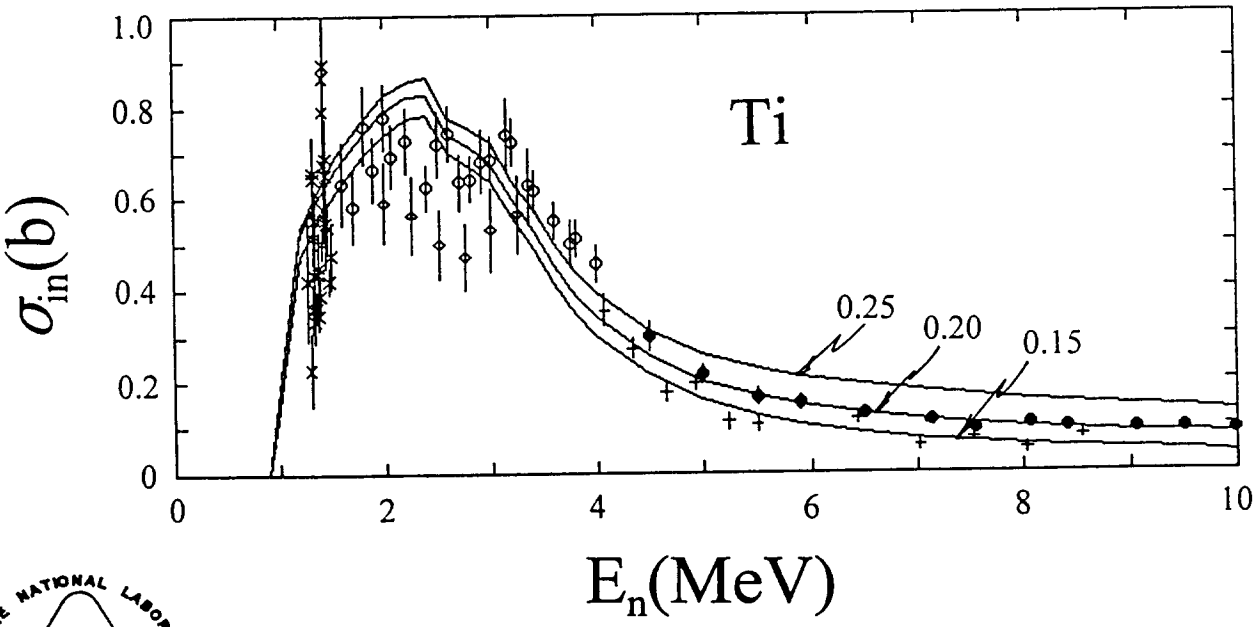

ARGONNE NATIONAL LABORATORY, ARGONNE, ILLINOIS
Operated by THE UNIVERSITY OF CHICAGO
for the U. S. DEPARTMENT OF ENERGY
under Contract W-31-109-Eng-38

Argonne National Laboratory

Argonne National Laboratory, with facilities in the states of Illinois and Idaho, is owned by the United States Government, and operated by the University of Chicago under provisions of a contract with the Department of Energy.

Disclaimer

Reproduced from the best available copy.

Available to DOE and DOE contractors from the Office of Scientific and Technical Information, P. O. Box 62, Oak Ridge, TN 37831; prices available from (423) 576-8401.

Available to the public from the National Technical Information Service, U. S. Department of Commerce, 5285 Port Royal Road, Springfield, VA 22161.

PUBLICATIONS IN THE ANL/NDM SERIES

A listing of recent issues in this series is given below. Issues and/or titles prior to ANL/NDM-120 can be obtained from the National Technical Information Service, U. S. Department of Commerce, 5285 Port Royal Road, Springfield, VA 22161, or by contacting the author of this report at the following address:-

Technology Development Division
Argonne National Laboratory
9700 South Cass Avenue
Argonne, IL 60439
USA

A. B. SMITH, P. T. GUENTHER, J. F. WHALEN, AND S. CHIBA
Fast-neutron Total and Scattering Cross Sections of ^{58}Ni and Nuclear Models
ANL/NDM-120, July 1991

S. CHIBA AND D. L. SMITH
A Suggested Procedure for Resolving an Anomaly in Least-squares Data Analysis Known as "Peelle's Pertinent Puzzle" and the General Implications for Nuclear Data Evaluation
ANL/NDM-121, September 1991

D. L. SMITH AND DOMINIQUE FEAUTRIER
Development and Testing of a Deuterium Gas Target Assembly for Neutron Production Via the H-2(D,N)HE-3 Reaction at a Low-energy Accelerator Facility
ANL/NDM-122, March 1992

D. L. SMITH AND E. T. CHENG
A Review of Nuclear Data Needs and Their Status for Fusion Reactor Technology with some Suggestions on a Strategy to Satisfy the Requirements
ANL/NDM-123, September 1991

J. W. MEADOWS
The Thick-Target $^{9}Be(d,n)$ Neutron Spectra for Deuteron Energies Between 2.6 and 7.0-MeV
ANL/NDM-124, November 1991

A. B. SMITH AND P. T. GUENTHER
Fast-Neutron Scattering Near Shell Closures:- Scandium
ANL/NDM-125, August 1992

A. B. SMITH, J. W. MEADOWS AND R. J. HOWERTON
A Basic Evaluated Neutronic Data File for Elemental Scandium
ANL/NDM-126, November 1992

A. B. SMITH AND P. T. GUENTHER
Fast-Neutron Interaction With Vibrational Cadmium Nuclei
ANL/NDM-127, November 1992

D. L. SMITH
A Least-Squares Computational "Tool Kit"
ANL/NDM-128, April 1993

JOSEPH McCABE, A. B. SMITH AND J. W. MEADOWS
Evaluated Nuclear Data Files for the Naturally-Occurring Isotopes of Cadmium
ANL/NDM-129, June 1993

A. B. SMITH AND P. T. GUENTHER
Fast-Neutron Interaction with the Fission Product ^{103}Rh
ANL/NDM-130, September 1993

A. B. SMITH AND P. T. GUENTHER
Fast-Neutron Scattering from Vibrational Palladium Nuclei
ANL/NDM-131, October 1993

A. B. SMITH
Neutron Interaction with Doubly-Magic ^{40}Ca
ANL/NDM-132, December 1993

A. B. SMITH
Neutron Scattering at Z = 50:- Tin
ANL/NDM-133, September 1994

A. B. SMITH, S. CHIBA AND J. W. MEADOWS
An Evaluated Neutronic File for Elemental Zirconium
ANL/NDM-134, September 1994

A. B. SMITH
Neutron Scattering from Elemental Uranium and Thorium
ANL/NDM-135, February 1995

A. B. SMITH
Neutron Scattering and Models:- Iron
ANL/NDM-136, August 1995

A. B. SMITH
Neutron Scattering and Models:- Silver
ANL/NDM-137, July 1996

A. B. SMITH
Neutron Scattering and Models:- Chromium
ANL/NDM-138, June 1996

W. P. POENITZ AND S. E. AUMEIER
The Simultaneous Evaluation of the Standards and Other Cross Sections of Importance for Technology
ANL/NDM-139, September 1997

JASON T. DALY AND DONALD L. SMITH
A Compilation of Information on the $^{31}P(p,\gamma)^{32}S$ *Reaction and Properties of Excited Levels in* ^{32}S
ANL/NDM-140, November 1997

A. B. SMITH
Neutron Scattering and Models:- Titanium
ANL/NDM-141, July 1997

A. B. SMITH
Neutron Scattering and Models:- Molybdenum
ANL/NDM-142, to be published.

ROY E. MILLER AND DONALD L. SMITH
A Compilation of Information on the $^{32}S(p,\gamma)^{33}Cl$ *Reaction and Properties of Excited Levels in* ^{33}Cl
ANL/NDM-143, to be published.

ROY E. MILLER AND DONALD L. SMITH
A Compilation of Information on the $^{31}P(p,\alpha)^{28}Si$ *Reaction and Properties of Excited Levels in* ^{28}Si
ANL/NDM-144, to be published.

ANL/NDM-141

NEUTRON SCATTERING AND MODELS:- TITANIUM*

by

A. B. Smith

Argonne National Laboratory
Argonne, Illinois
and
The University of Arizona
Tucson, Arizona

July, 1997

Keywords:
Measured $d\sigma/d\Omega_{el}$ and $d\sigma/d\Omega_{inel}$ (1.5 → 10 MeV) for neutrons incident on elemental silver. Comprehensive optical and coupled-channels model interpretations.

---

* This work supported by the United States Department of Energy under contract W-31-109-Eng-38, and by the Nuclear and Energy Engineering Program, College of Engineering and Mines, University of Arizona.

TABLE OF CONTENTS

ANL/NDM-141

NEUTRON SCATTERING AND MODELS:- TITANIUM

by

A. B. Smith

Argonne National Laboratory
Argonne, Illinois
and
The University of Arizona
Tucson, Arizona

July, 1997

ABSTRACT

Differential neutron elastic-scattering cross sections of elemental titanium were measured from 4.5 → 10.0 MeV in incident-energy increments of ≈ 0.5 MeV. At each energy the measurements were made at forty or more scattering angles distributed between ≈ 17^{o} and 160^{o} degrees. Concurrently, differential neutron inelastic-scattering cross sections were measured for observed excitations of 0.975±0.034, 1.497±0.033, 2.322±0.058, 3.252±0.043, 3.700±0.093, 4.317±0.075 and 4.795±≈0.100 MeV. All of the observed inelastically-scattered neutron groups were composites of contributions from several isotopes and/or levels. The experimental results were used to develop energy-average optical, statistical and coupled-channels models.

1. Introduction

Elemental titanium consists of the five isotopes ^{46}Ti(8%), ^{47}Ti(7.3%), ^{48}Ti(73.8%), ^{49}Ti(5.5%) and ^{50}Ti(5.4%). All of them are $f_{7/2}$ nuclei. In particular, ^{50}Ti is a $(\pi f_{7/2})^2$ configuration, magic in neutron number. The prominent isotope, ^{48}Ti, is probably a $(\pi f_{7/2})^2(\nu f_{7/2})^{-2}$ configuration, an assumption which is strongly supported by observed M1 and E2 transitions [Law80]. All of the even isotopes have a yrast 2^+ level at ≈ 1 to 1.5 MeV [NDS]. There is a low-lying level in ^{47}Ti (159 keV, $7/2^-$), but subsequent excitations are well above an MeV [NDS] and the isotope is of low abundance. ^{49}Ti has no excited levels below ≈ 1.4 MeV and the isotope is of very low abundance. Thus elemental titanium is reasonably represented by an even-even $f_{7/2}$ collective nucleus with a yrast 2^+ level at approximately an MeV. The even titanium isotopes are in a region where the 2^+ levels are classic vibrators [Adl+56, SW55]. Charged-particle (α-particle and proton) studies indicate a strong collective vibrational interaction (e.g., [Lut+69, Lut+74, Err67, SBD63, Per+70, Ber+68, YS67 and NDS]) with a β_2 for the excitation of the yrast 2^+ one-phonon quadrupole state of ≈ 0.22, and approximately the same β_2 values for the excitation of the two-phonon quadrupole states. In addition, octupole states have been reported above excitations of ≈ 3 MeV with β_3 values of 0.15 → 0.20. Thus it is reasonable to expect that the incident neutron to have a relatively strong vibrational interaction with a proton core. Such an expectation is supported by the results of coulomb-excitation studies [Ram+87]. The targets are near shell closures and thus it is reasonable to interpret the observations in the context of the core-coupling model [MBA75]. The neutron interaction with titanium was not well known. The body of the experimental information was obtained at incident energies of less than ≈ 4 MeV, much of it by the author and his associates. There is some knowledge of elastic and inelastic scattering from titanium at energies of ≈ 4 → 8 MeV [KP73], and several very old elastic-scattering measurements at ≈ 14 MeV. There appear to be no neutron scattering results above ≈ 14 MeV, and very little information above ≈ 8.5 MeV. Even the neutron total cross sections were essentially unknown above ≈ 15 MeV until very recent measurements [Hai+96]. At the lower energies the entire neutron interaction with titanium is subject to large fluctuations from partially resolved resonance effects. Furthermore, titanium lies near the peak of the 3S resonance in the s-wave strength function. It is a region where the neutron processes tend to have an anomalous behavior, and one where

dispersive effects may well be substantive.

The present work had the objective of new understanding of the neutron interaction with titanium from basic and applied points of view. Titanium is a light, durable, strong, and high-temperature metal widely used in areo-space, fusion and other applications. Thus its neutronic properties may be of interest in a number of contexts. The following sections of this paper deal with:- 2) the experimental method, 3) experimental results, 4) extensive modeling of the measured values, and 5) physical consequences of the measurements and models.

2. Experimental Methods

All of the measurements were made using the fast-neutron time-of-flight method [CL55] and the Argonne ten-angle detection system. This method and apparatus have been amply described elsewhere [Smi+92] and therefore only a general outline and details specific to the present measurements are given here.

The measurement sample was a cylinder of high-purity metallic elemental titanium 2 cm in diameter and 2 cm long. The measured density of the sample was very similar to that reported in the literature for the elemental metal. The neutron source was the $D(d,n)^3He$ reaction. The target deuterium gas was contained in an $\approx$ 2 cm long gas cell at a pressure providing energy spreads of $\approx$ 300 keV at 4 MeV, decreasing to $\approx$ 100 keV at 10 MeV [Dro87]. The mean neutron energy was determined to within $\approx$ 10 keV by control of the incident ion beam. The neutron source was pulsed at a 2 MHz repetition rate with a burst duration of $\approx$ 1 nsec. Incident deuterium peak-pulsed currents were more than ten mA, obtained using a double-harmonic klystron-bunching system associated with a tandem accelerator. The scattering sample was placed $\approx$ 15 cm from the neutron source. Ten scattered-neutron flight paths $\approx$ 5 m long were arranged about the sample in a massive shielding system. The relative scattering angles were optically determined to $\approx 0.1^{o}$, and the absolute calibration of the angular system was established to approximately the same precision by observing neutron scattering from a heavy sample either side of the center line at angles where the cross section changes very rapidly with angle. Ten hydrogenous liquid scintillators were placed at the ends of the flight paths. These detectors were $\approx$ 4 cm thick and 12.5 cm in diameter. The relative energy sensitivity of each of these detectors was experimentally determined by observation of the well known spectrum of neutrons emitted at the spontaneous fission of ^{252}Cf, and extrapolated above 8 MeV using Monte-Carlo modeling [SGS77]. Two additional time-of-flight detectors were arranged to monitor the neutron source intensity. Pulse-shape-sensitive circuitry suppressed the gamma-ray response of the neutron detectors. Twelve timing channels were employed with a digital computer to concurrently measure the time-of-flight of the neutrons from the

source to each of the detectors. This data acquisition system was integrated with the subsequent digital data processing programs so as to provide an efficient flow of the large volumes of data. The titanium scattering cross sections were determined relative to the H(n,n) scattering standard [CSL83] using a polyethylene (CH_2) sample identical in size to the titanium sample. All of the titanium cross-section measurements and the H(n,n) calibration measurements were corrected for beam-attenuation, multiple-event and angular-resolution effects using Monte-Carlo techniques [Smi91].

3. Experimental Results

3.1. Neutron Elastic Scattering

The elastic-scattering measurements were made from 4.5 to 10 MeV in increments of 0.5 MeV, and at forty or more scattering angles at each incident-energy, distributed between ≈ 17^{o} and 160^{o}. The experimental resolution was sufficient to define the elastic scattering processes in all of the naturally-occurring isotopes except for contamination due to inelastic scattering resulting from the excitation of the 159 keV $7/2^{+}$ state in ^{47}Ti [NDS]. That isotope is only 7.3% abundant and the relevant inelastic cross section is modest, so the distortion of the elemental elastic-scattering results is small (< 1 mb/sr) and was ignored throughout this work. The elastic-scattering results are summarized in Fig. 3.1.1. The uncertainties in these differential values range from ≈ 3%, including systematic and statistical contributions, in regions of appreciable cross section to larger values in the minima of the distributions. These uncertainties are indicated in Fig. 3.1.1. There is very little previously-reported titanium elastic-scattering information comparable with the present results. There are a few distributions from the work of Kinney and Perey [KP73] which are reasonably consistent with the present results as indicated in Fig. 3.1.2, particularly considering that the two sets of data were not obtained at exactly the same energies and the cross sections can be expected to fluctuate with energy. There are some lower-energy elastic-scattering results, notably the work of refs. [Smi+78 and Gue+78], that reasonably extrapolate to the present values. However, at lower energies fluctuations are even more of a concern.

3.2. Neutron Inelastic Scattering

The inelastic-scattering measurements were made currently with the elastic-scattering determinations. Eight inelastically-scattered neutron groups were observed corresponding to measured excitation energies of 975±34, 1497±33, 2322±58, 3252±43, 3700±93, 4317±75 and 4795±100 keV (where the cited uncertainties are the rms deviations from the means of a

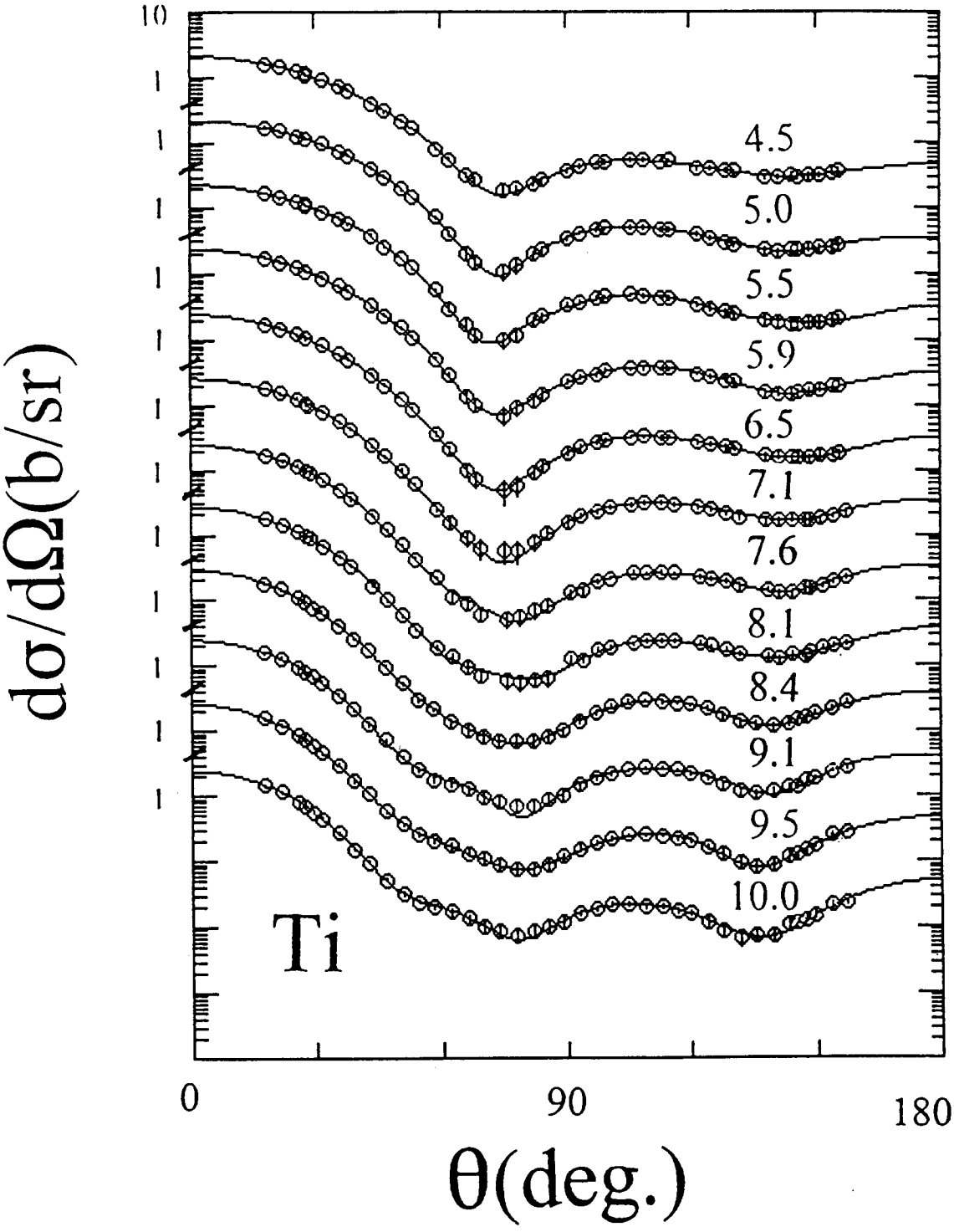

Fig. 3.1.1. Measured differential elastic-scattering cross sections of elemental titanium. Circular symbols indicate the present experimental values and curves the results of fitting Legendre-polynomial series to the measured cross sections. Approximate incident energies are numerically noted in MeV. Throughout this work angular distributions are illustrated in the laboratory coordinate system.

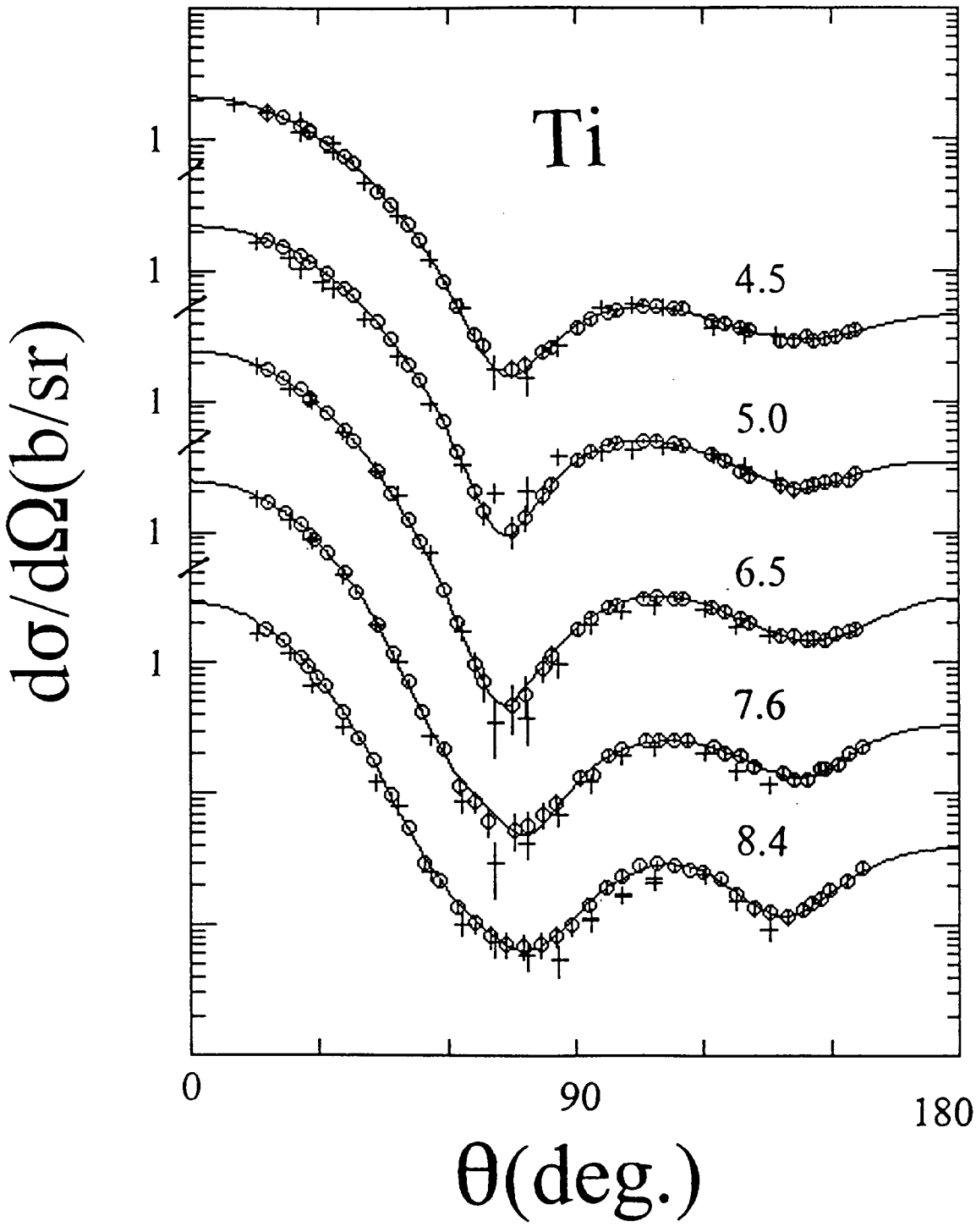

Fig. 3.1.2. Comparisons of measured elemental titanium elastic-scattering cross sections. Circular symbols indicate the present results and crosses the values from ref. [KP73]. Approximate incident energies are noted in MeV and curves indicate results of Legendre fitting the present values.

number of measurements and not necessarily the experimental resolution). All of these observed neutron groups were associated with contributions from more than one level in the naturally occurring isotopes of titanium, and in many cases with a number of components, as indicated in Table 3.2.1. The cross sections for some of these groups were very well defined at many angles and incident energies. In other cases the observations were not as clear nor made at as many angles and/or energies. The excitation of the 975 keV "level" was best defined, with the corresponding differential cross sections shown in Fig. 3.2.1. At the lower energies these distributions tend towards isotropy, but as the incident energy increases they increasingly peak forward. Similar information in the literature is largely confined to ref. [KP73]. That data is compared with the present results for the excitation of the 975 keV "level" in Fig. 3.2.2. There are differences, but the values of ref. [KP73] tend to support those of the present work.

The observed neutron groups corresponding to higher excitations were not as well defined as that of the 975 keV group, but tended to be isotropically distributed with angle. All of the observed inelastic-neutron distributions were fitted with Legendre-polynomial expansions to obtain the angle-integrated inelastic-scattering cross sections. The latter values are illustrated in Fig. 3.2.3. This figure also makes comparison with (n,n') values reported in the literature in those cases where the incident and scattered neutron resolutions are reasonably comparable [KP73, Ram75, Bar+74]. The comparisons are difficult in these complex situations, but generally the present results are reasonably consistent with those of ref. [KP73], and also extrapolate to the earlier and lower-energy results obtained at this laboratory [Gue+78, Smi+78]. There are some (n;n',γ) experimental results reported in the literature. Comparison of (n;n',γ) and (n,n') values is difficult due to branching ratios, internal conversion and isotopic complexity and therefore was not attempted.

4. Model Interpretations

4.1. Data Base

The model interpretations were primarily based upon the observed differential elastic-scattering distributions. These will fluctuate very sharply with energy below several MeV (e.g., see ref [Bar+74]) and thus averages of the observed distributions must be used up to a number of MeV. Below 1.5 MeV $\approx$ 250 keV averages of the elastic scattering of Barnard et al. [Bar+74] were used. Even in these broad averages fluctuations obviously persisted. From 1.5 to 4.0 MeV $\approx$ 200 keV averages of the elastic-scattering results of Smith et al. [Smi+78 and Gue+78] were used. These data are in considerable energy and angle detail. From 4.0 to 10 MeV the present elastic-scattering

Table 3.2.1. Comparison of observed titanium excitation energies with levels reported in the literature [NDS].

E_x(keV)	Reported Levels				
Observed	^{46}Ti	^{47}Ti	^{48}Ti	^{49}Ti	^{50}Ti
975±34	889(2+)	-----	984(2+)	-----	-----
1497±33	-----	1250(1/2-) 1252(9/2-) 1444(11/2-) 1550(3/2-) 1671(?) 1794(1/2-) 1825(3/2+)	-----	1382(3/2-) 1542(11/2-) 1585(3/2-) 1623(5/2-) 1723(1/2-) 1762(5/2-)	1354(2+)
2322±58	2010(4+) 2611(0+)	many	2296(4+) 2421(2+) (2465?)	many	2675(4+)
3252±43	2962(2+) 3058(3-) 3168(1-) 3213(?) 3236(2+) 3299(6+) 3338(?)	many	2997(0+) 3062(2+) 3224(3+) 3240(4+) 3333(6+) 3358(3-) 3370(2+)	many	3198(6+)
3700±93	many	many	many	many	many
4317±75	many	many	many	many	many
4795±100	many	many	many	many	many

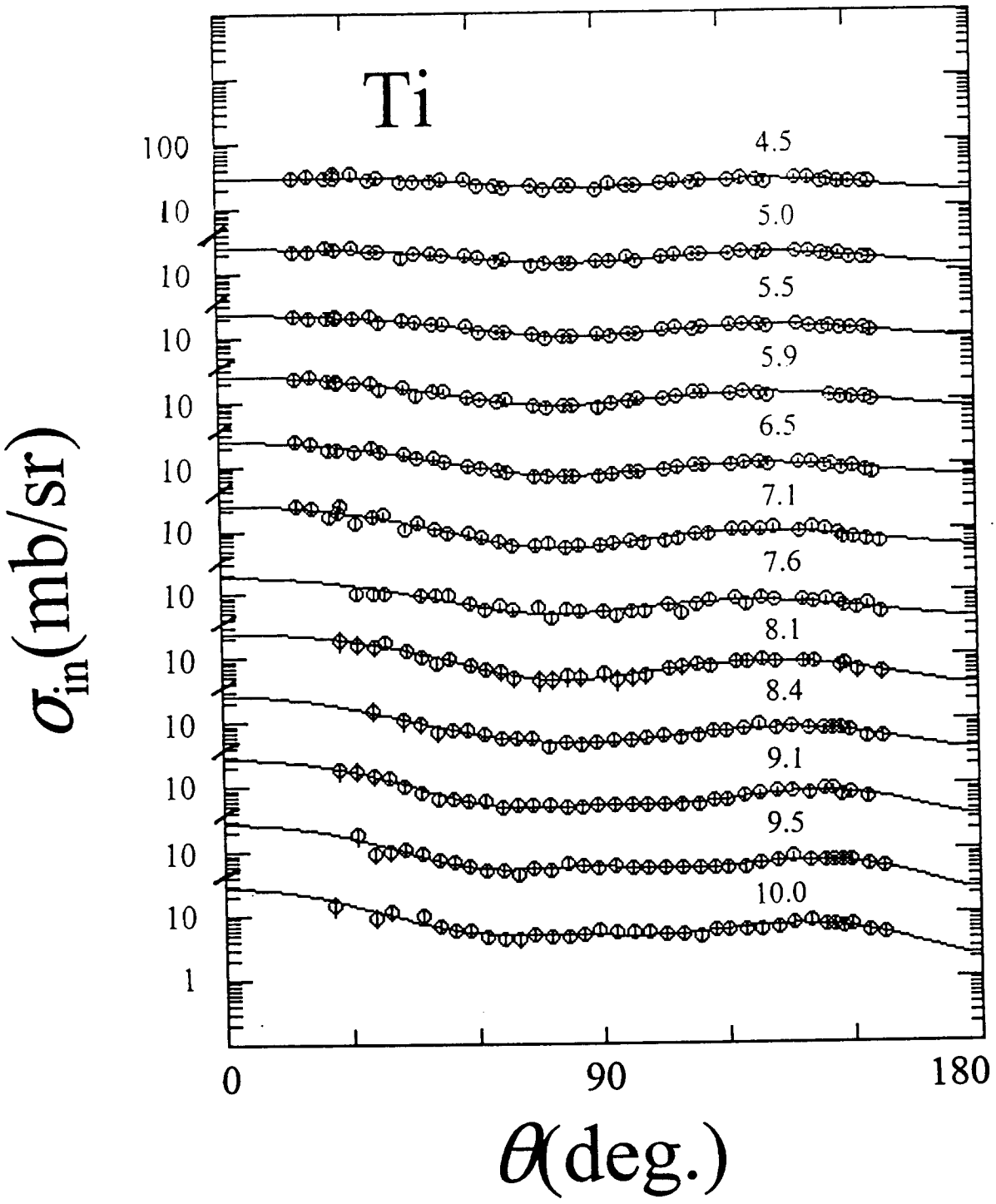

Fig. 3.2.1. Elemental titanium cross sections for the observed inelastic excitation of the 975 keV level. The present experimental results are indicated by symbols and curves denote the results of Legendre-polynomial fitting. Approximate incident energies are numerically noted in MeV.

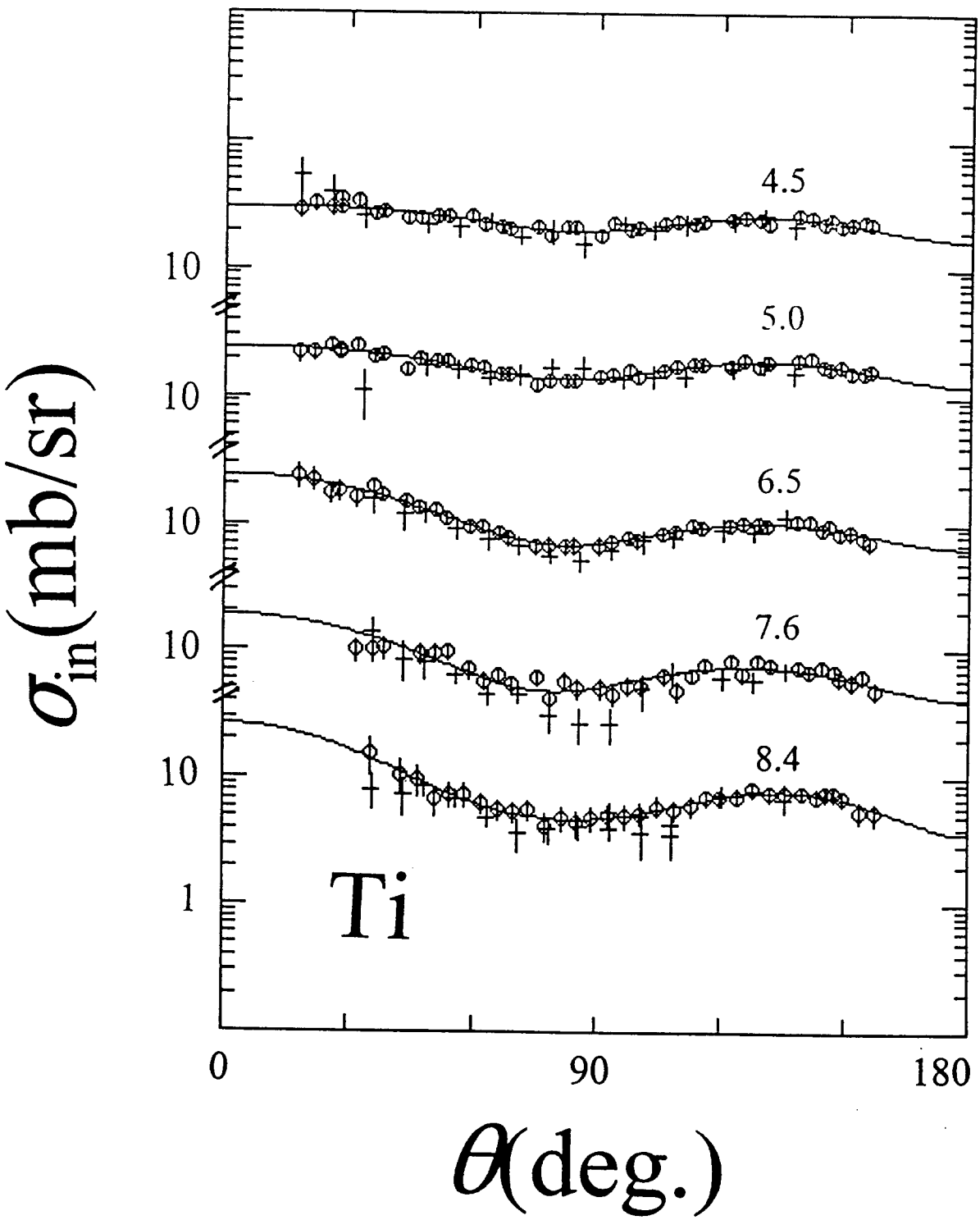

Fig. 3.2.2. Comparisons of measured elemental differential cross sections for the excitation of the ≈ 975 keV level in titanium. The present experimental results are indicated by circular symbols and those from ref. [KP73] by crosses. Curves indicate the results of fitting the present values with Legendre-polynomial series. Approximate incident energies are numerically noted in MeV.

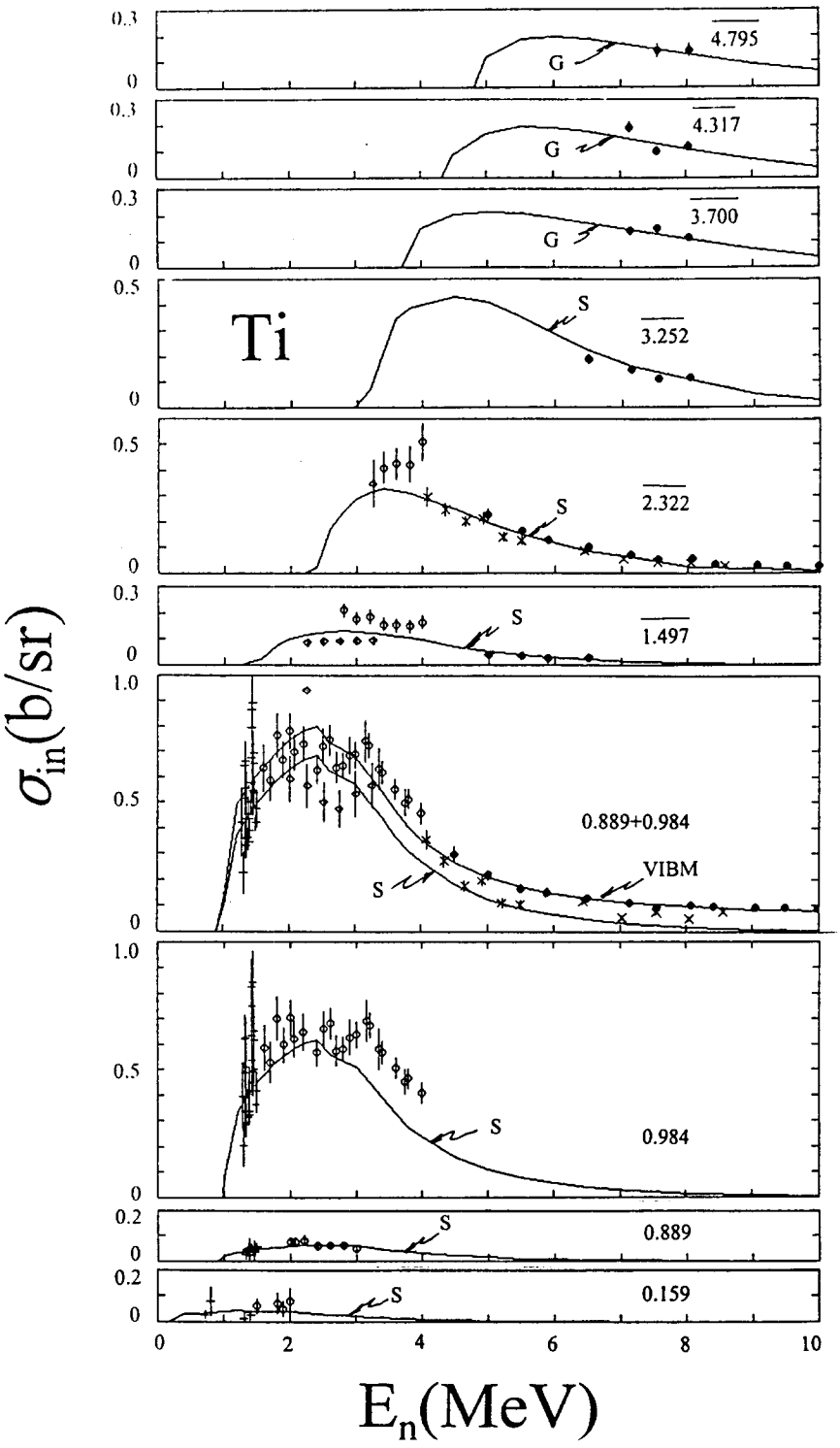

Fig. 3.2.3. Angle-integrated inelastic-scattering cross sections of elemental titanium. The present results are indicated by solid circular symbols, lower-energy results from this laboratory [Smi+78] by open circular symbols, results from ref. [KP73] by "X" symbols, "diamond symbols" the results of ref. [Ram75] and "+" symbols the results of ref. [Bar+74]. Curves indicate:- "S" spherical model calculations, "VIBM" vibrational model calculations, and "G" eyeguides. Excitation energies are noted in keV.

results were used. The single ≈ 14 MeV elastic-scattering distribution of ref. [SML59] was used. No higher-energy elastic-scattering information appears to be available. Consideration was also given to inelastic scattering, primarily associated with the excitation of the 984 keV level in ^{48}Ti, in both a differential and integral context. The inelastic scattering data was taken from the present work, that of Kinney and Perey [KP73], and the lower-energy inelastic studies of Barnard et al. [Bar+74], Ramstrom [Ram75], and of Smith et al. [Gue+78]. There are a few other scattering distributions reported in the literature but they do not have the energy and/or angle detail to substantively assist in the model derivations and thus they were not used. It is noted that the large majority of the knowledge of fast-neutron scattering from titanium emanates from the Argonne program over a period of approximately 20 years.

Additional attention was given to energy averages of the elemental neutron total cross sections, up to energies of ≈ 20 MeV, using the results of refs. [Hai+96, SSH74, FG71, Bar+74, GRH71, Smi+78, Gue+78, CW55, BBN62, Las51, CGB52, Goo52, Dju72, Goo+66]. Well into the MeV range these total cross sections display very large resonance fluctuations that are not consistent with energy-averaged models. Therefore, the experimental values were averaged over 50 keV below 1 MeV, over 100 keV at energies between 1 and 5 MeV, and over 200 keV at energies above 5 MeV. Even in these averages fluctuations persisted at lower energies. s- and p-wave neutron strength functions were compared with model predictions using the experimentally-based compilation of ref. [MDH81], and some attention was given to the polarization of elastically-scattered neutrons as reported in refs. [FWW66] and [ZJ74].

4.2. Potential Forms

All of the present models employed:- i) a Saxon-Woods (SW) real potential, ii) a SW-derivative surface-imaginary potential, iii) a spin-orbit potential (assumed real and non-deformed) of the Thomas form, and iv) where appropriate, a volume absorption of the SW form having the same geometry as the SW real potential [Hod71]. Throughout this study the parameters of the spin-orbit potential were taken from the model of Walter and Guss [WG86].

4.3. The Spherical Optical Model

All of the models described here were primarily derived from chi-square fitting the above elastic-scattering data base, with additional comparisons with inelastic-scattering processes, the total cross section and with strength functions. Two versions of the spherical optical model (SOM) were deduced. The simplest of these assumed that elemental titanium consisted entirely of ^{48}Ti (73.8% abundant) and is termed the "isotopic SOM", or ISOM. The more complex alternative concurrently considered contributions

from all five of the isotopes of the element, and is termed the "elemental SOM" or ESOM. All of the SOM calculations included contributions from compound-nucleus (CN) processes using the discrete-level properties given in ref. [NDS]. These contributions consisted of 12 levels in ^{46}Ti to excitations of ≈ 3.6 MeV, 14 in ^{47}Ti to ≈ 2.5 MeV, 14 in ^{48}Ti to ≈ 3.7 MeV, 11 in ^{49}Ti to ≈ 2.7 MeV, and 8 to excitations of ≈ 4.2 MeV in ^{50}Ti. Higher-energy CN excitations were estimated using the statistical model and parameters of Gilbert and Cameron [GC65]. All the CN calculations used the statistical formulation of Hauser and Feshbach [HF52], corrected for resonance width fluctuation and correlation effects following Moldauer [Mol80]. All of the SOM calculations were carried out using versions of the spherical optical model code ABAREX [Mol82]. Where appropriate, the calculations combined CN contributions from the g.s. and first-excited state in ^{47}Ti so as to be consistent with the experimental resolution. The fitting of the elastic distributions followed a five-step process given by; i) six parameter fitting varying real and imaginary strengths, radii and diffusenesses to obtain the real diffuseness (a_v), ii) five parameter fitting with a_v fixed to obtain the real radius (r_v), iii) four parameter fitting giving the imaginary radius (r_w), iv) three parameter fitting yielding the imaginary diffuseness (a_w), and finally v) two parameter fitting giving the real and imaginary potential strengths (J_v and J_w). This fitting regime has been widely used by the author [Smi+92]. It has the advantage of avoiding a bias due to initial parameter estimates but, on the other hand, is sensitive to the well-known correlations of real-potential depth and radius, and of imaginary-potential depth and diffuseness. In addition, the starting points of the fitting procedure were iterated over several cycles. Throughout this work the radii are given in the reduced form (r_i) where the full radius $R_i = r_i \cdot A^{1/3}$, and the potential strengths are given as volume-integrals-per-nucleon (J_i), unless otherwise explicitly noted.

The parameters of the ISOM and ESOM models, deduced in the above manner, are given in Tables 4.3.1 and 4.3.2, respectively. Throughout this work, potential parameters are given to sufficient precisions to make possible accurate reproduction of the calculations. The precisions do not necessarily imply parameter uncertainties, which are more realistically indicated by three significant figures. Results calculated with these potentials are compared with the elastic-scattering data base from which they were primarily developed in Figs. 4.3.1 and 4.3.2. Inelastic-scattering cross sections calculated with the ESOM are compared with the angle-integrated inelastic cross sections in Fig. 3.2.3. ESOM and ISOM total cross sections are

compared with the experimental values from a number of references in Fig. 4.3.3. In the latter comparisons the present spherical potentials were extrapolated above 14 MeV assuming the geometries and the imaginary potential strength are fixed at the 14 MeV values (this is a rather crude approximation). Finally, s- and p-wave strength functions calculated with the ISOM and ESOM are given in Table 4.3.3

4.4. The Coupled-Channels Model

Several simplifying assumptions were made in the coupled-channels model (CCM) treatment. It was assumed that the target was ^{48}Ti. The low-lying structure of that isotope is very similar to that of ^{46}Ti, and the two combined amount to ≈ 82% of the element. The target was assumed to be a collective nucleus, either a simple one-phonon vibrator or a prolate rotor, with a β_2 as defined by Tamura [Tam65]. Herein the vibrational and rotational models are referred to as the VIBM and ROTM, respectively. With the above simplification, the model derivations followed the procedures outlined above for the SOM. All of the calculations employed the coupled-channels code ECIS96 [Ray96]. Seven independent fitting procedures were followed for both the VIBM and ROTM, corresponding to assumed values of β_2 of 0.01, 0.05, 0.10, 0.15, 0.20, 0.25 and 0.30. These β_2 values extend over a reasonable range. As discussed in Section 5, β_2 = 0.20 was chosen as most appropriate for both the VIBM and ROTM. With that β_2 value, the VIBM and ROTM parameters of Tables 4.4.1 and 4.4.2, respectively, were obtained. The elastic-scattering results obtained with the VIBM and ROTM are compared with the experimental data base in Figs. 4.4.1 and 4.4.2, respectively. Fig. 4.4.3 compares measured neutron total cross sections with those calculated with the VIBM and ROTM. Figs. 4.4.4 and 4.4.5 compare the experimental cross sections for the excitation of the yrast 2^+ 984 keV level with those calculated with the VIBM and ROTM, respectively. Table 4.3.3 includes VIBM and ROTM strength functions.

Some of the physical implications of these models are discussed in Section 5, below.

5. Discussion and Summary

A comparison of the parameters of the ISOM (Table 4.3.1), ESOM (Table 4.3.2), VIBM (Table 4.4.1) and ROTM (Table 4.4.2) offers some guidance as to systematic trends, at least in the present context of neutron scattering from titanium. The a_v are

Table 4.3.1. Parameters for the spherical optical-model potential, ISOM. Geometries (a_i and r_i) are given in fermis and strengths (J_i) as volume-integrals-per-nucleon in units of MeV-fm^3, except for the spin-orbit potential where the potential depth (V_{so}) is given in MeV. Incident energy (E) is in MeV. There were two iterations on the parameters starting the fitting procedures.[+*]

Real Potential		
$J_v = 522.2 - 9.3064 \cdot E$		(447.7)
$r_v = 1.3816 - 0.015692 \cdot E$		(1.2561)
$a_v = 0.5809$		(0.5809)
Imaginary Potential		
$J_w = 95.6 - 3.092 \cdot E$		(70.8)
$r_w = 1.4253 - 0.03380 \cdot E$		(1.1549)
$a_w = 0.091 + 0.0870 \cdot E$	$(E \leq 9.06)$	(0.7870)
$= 0.8792$	$(E > 9.06)$	
Spin-Orbit Potential		
$V_{so} = 5.935 - 0.015 \cdot E$		(5.815)
$r_{so} = 1.103$		(1.103)
$a_{so} = 0.56$		(0.56)

* Herein the cited parameter precisions make possible accurate reproduction of the calculated values but do not necessarily reflect uncertainty.

\+ The values of the parameters at 8 MeV are given in parenthesis.

Table 4.3.2. Parameters for the spherical ESOM optical-model potential of the text. There were two iterations on the initial parameters used in the fitting procedures. The notation is identical to that of Table 4.3.1.

Real Potential

$J_v = 530.6 - 9.333 \cdot E$ (455.9)

$r_v = 1.3931 - 0.01511 \cdot E$ (1.2722)

$a_v = 0.5780$ (0.5780)

Imaginary Potential

$J_w = 104.2 - 3.902 \cdot E$ (73.0)

$r_w = 1.4380 - 0.03747 \cdot E$ (1.1382)

$a_w = 0.096 + 0.08236 \cdot E \quad (E \leq 10)$ (0.7549)

$= 0.9188 \quad (E > 10)$

Spin-Orbit Potential (Same as Table 4.3.1)

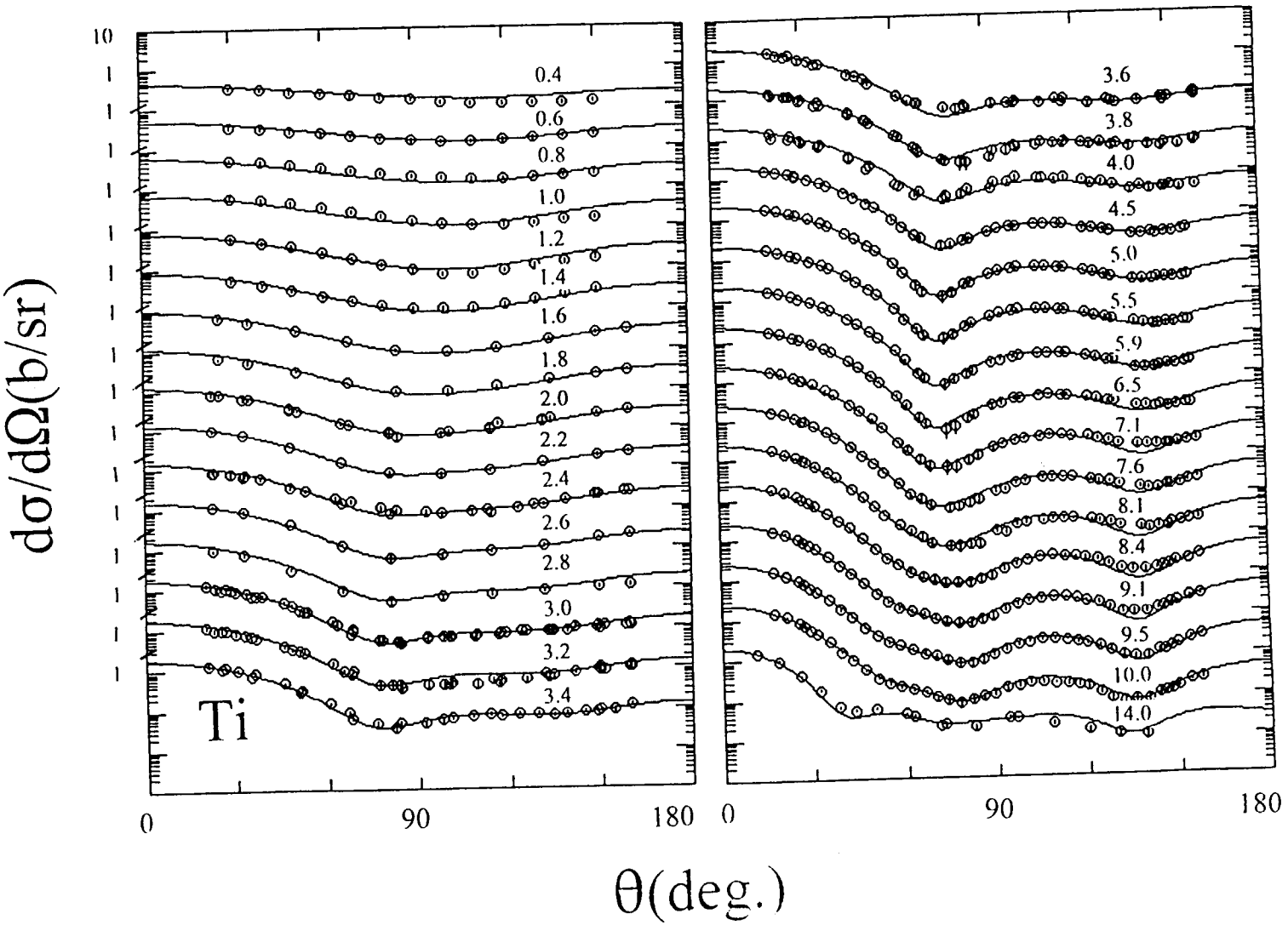

Fig. 4.3.1. Comparisons of measured and calculated elastic scattering cross sections. Data points indicate the experimental data base described in Section 4.1 of the text and the curves the results of ISOM calculations. Approximate incident neutron energies in MeV are numerically noted.

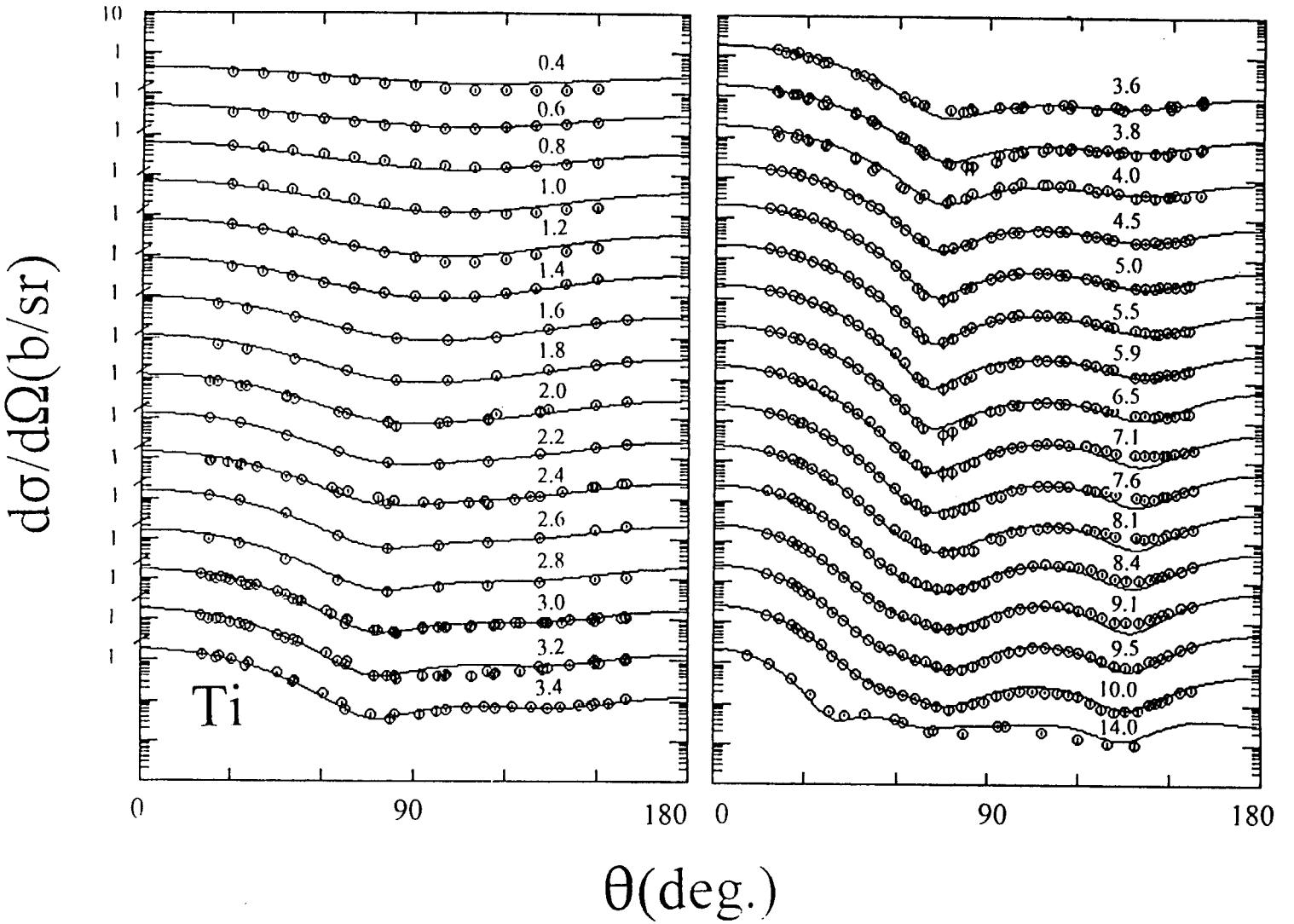

Fig. 4.3.2. Comparison of measured and calculated elastic scattering cross sections. The calculations used the ESOM, otherwise the notation is identical to that of Fig. 4.3.1.

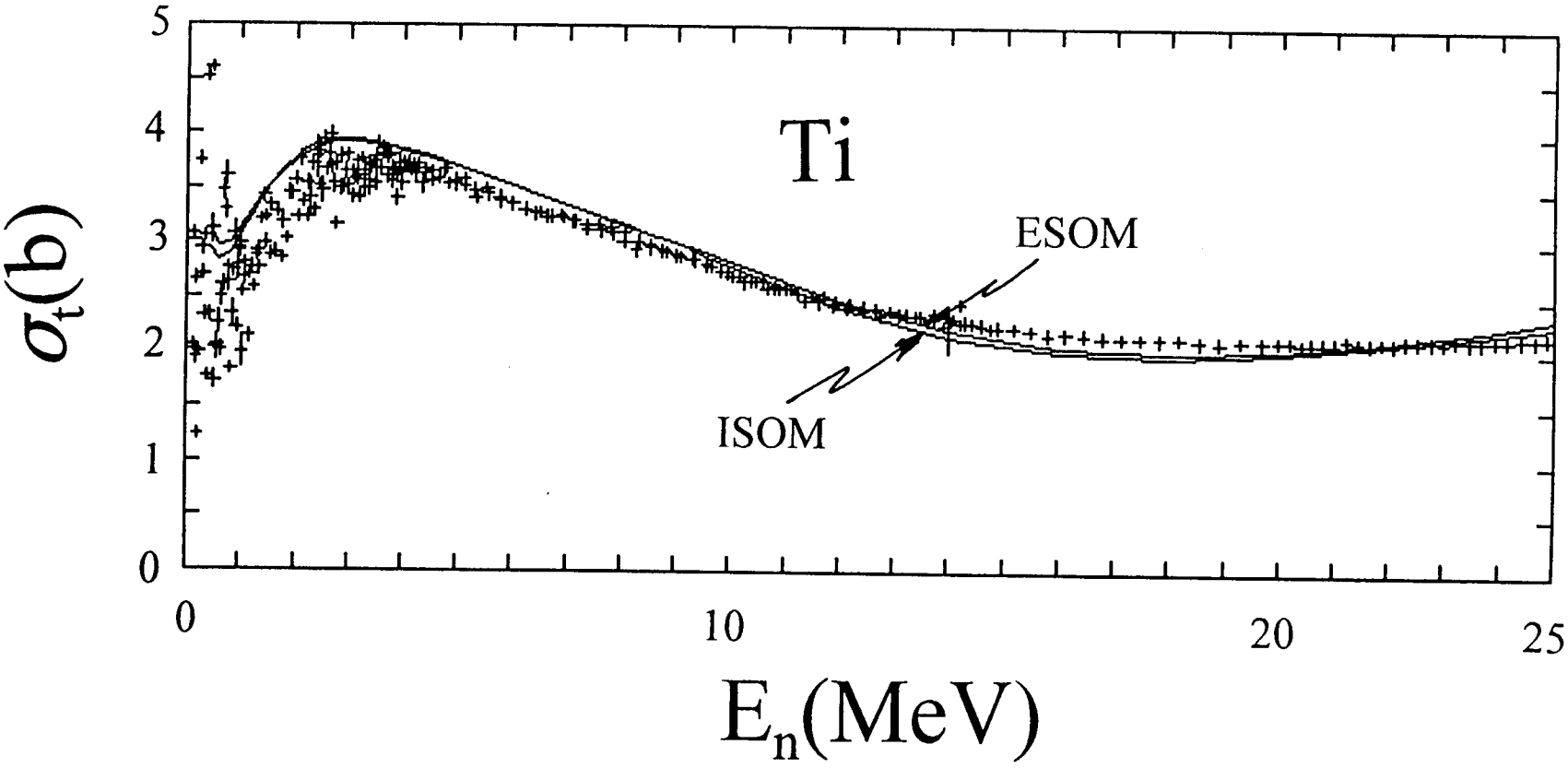

Fig. 4.3.3. Comparisons of measured and calculated neutron total cross sections. Experimental values are indicated by "+" symbols, as defined in Section 4.1 of the text. Curves indicate ISOM and ESOM results as noted.

Table 4.3.3. Calculated and measured strength functions in units of 10^{-4}.

Model	s-wave	p-wave
ISOM	3.660	0.931
ESOM	3.944	0.863
VIBM	4.225	1.558
2PVIBM	4.958	1.367
DVIBM	4.595	1.305
ROTM	4.800	1.797
Measurements		
Ref. [MDH81]	4.0±1.3	------

Table 4.4.1. Parameters for the VIBM potential with $\beta_2 = 0.20$. The notation is identical to that of Table 4.3.1. There were four iterations of the initial parameters used in the fitting procedure.

Real Potential

$J_v = 472.6 - 1.1896 \cdot E$ (463.1)

$r_v = 1.2716$ (1.2716)

$a_v = 0.6322$ (0.6322)

Imaginary Potential

$J_w = 54.8 - 0.2035 \cdot E$ (53.2)

$r_w = 1.3403 - 0.02050 \cdot E$ (1.1763)

$a_w = 0.284 + 0.06507 \cdot E \quad (E \leq 5)$ (0.6141)

$= 0.6141 \quad (E > 5)$

Spin-Orbit Potential (the same as Table 4.3.1)

Table 4.4.2. Parameters for the ROTM potential with $\beta_2 = 0.20$. The notation is identical to that of Table 4.3.1. Three iterations were made on the initial parameters in the fitting procedure.

Real Potential

$$J_v = 478.8 - 1.8044 \cdot E \qquad (464.4)$$

$$r_v = 1.2599 - 0.002888 \cdot E \qquad (1.2368)$$

$$a_v = 0.6420 \qquad (0.6420)$$

Imaginary Potential

$$J_w = 58.8 - 0.5477 \cdot E \qquad (54.4)$$

$$r_w = 1.2924 - 0.00924 \cdot E \qquad (1.2185)$$

$$a_w = 0.277 + 0.08285 \cdot E \quad (E \leq 4) \qquad (0.6000)$$
$$= 0.6000 \quad (E > 4)$$

Spin-Orbit Potential (the same as Table 4.3.1)

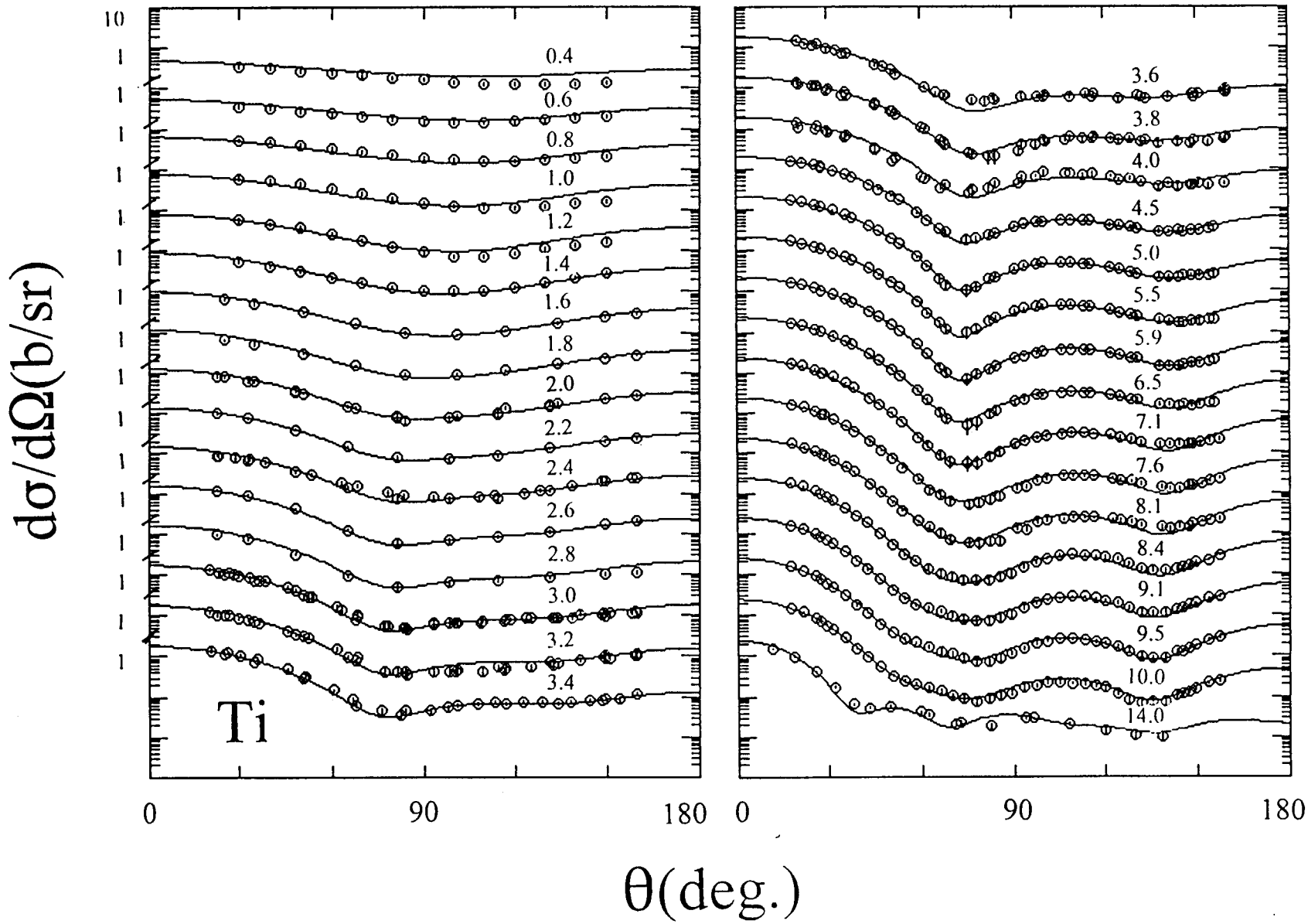

Fig. 4.4.1. Comparison of measured (symbols) and calculated (curves) differential elastic-scattering cross sections. The calculations employed the VIBM. The notation is identical to that of Fig. 4.3.1.

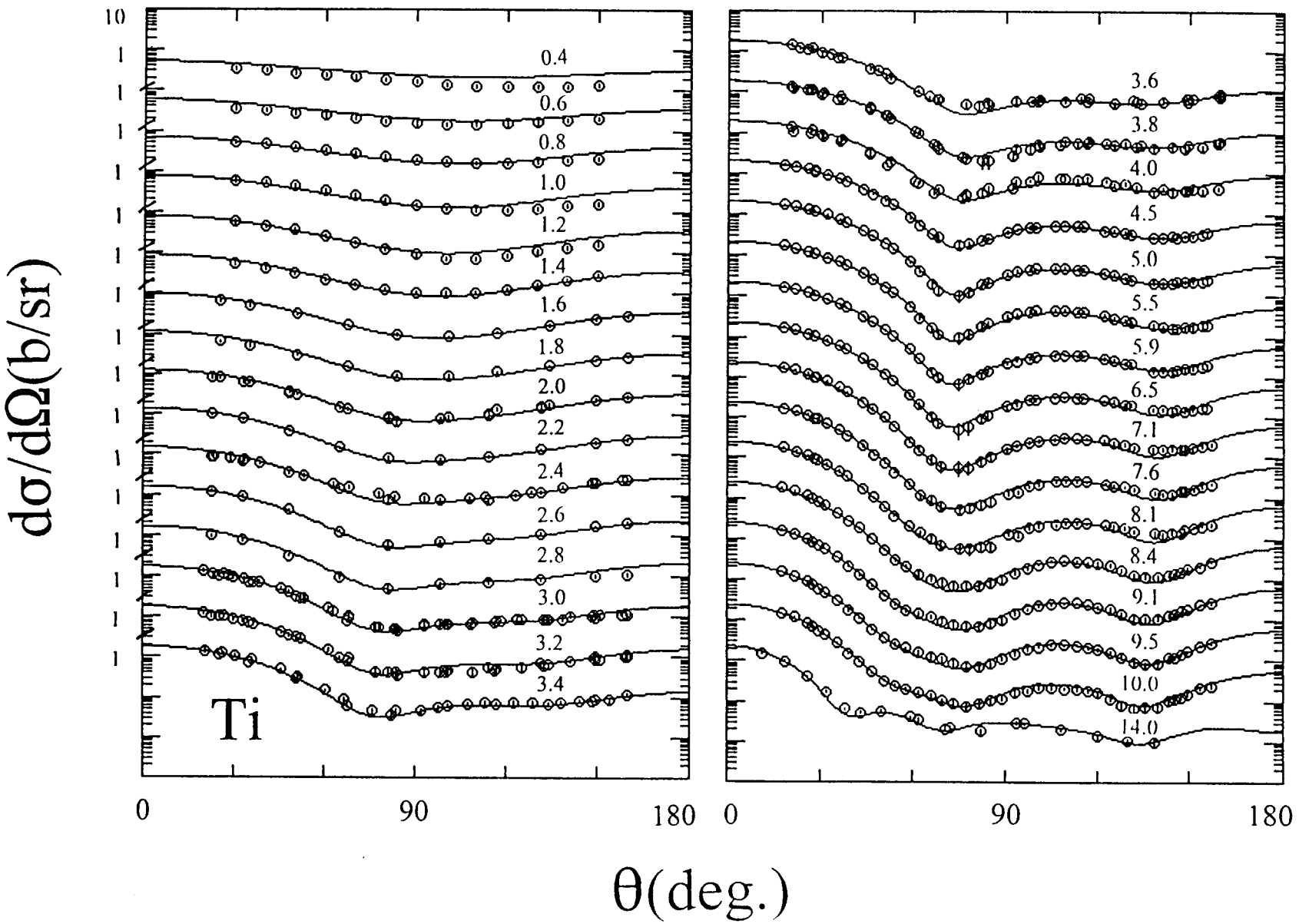

Fig. 4.4.2. Comparison of measured (symbols) and calculated (curves) differential elastic-scattering cross sections. The calculations employed the ROTM. Otherwise the notation is identical to that of Fig. 4.3.1.

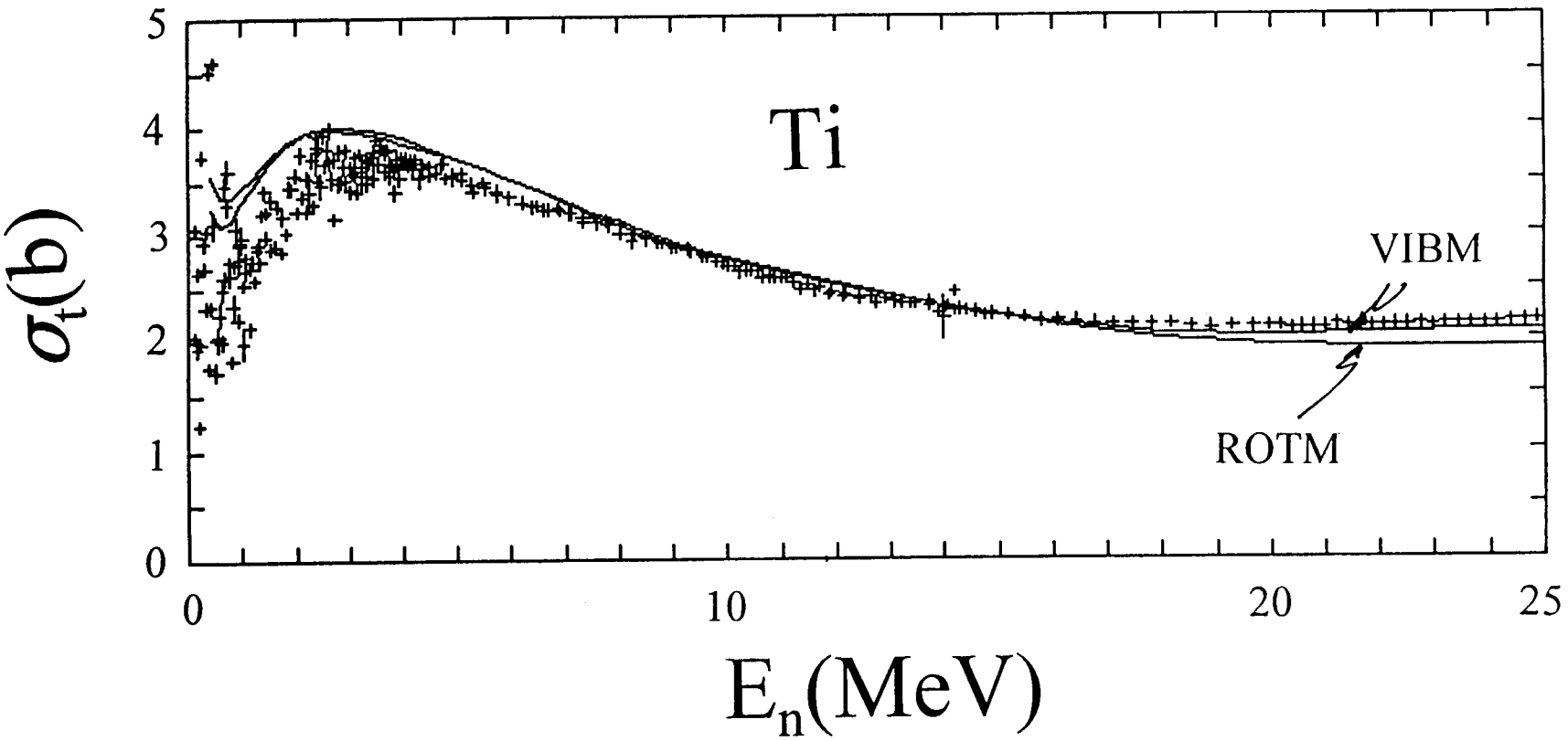

Fig. 4.4.3. Comparison of measured and calculated total cross sections. The "+" symbols indicate experimental values as specified in Section 4.1. Curves indicate the results of VIBM and ROTM calculations as noted.

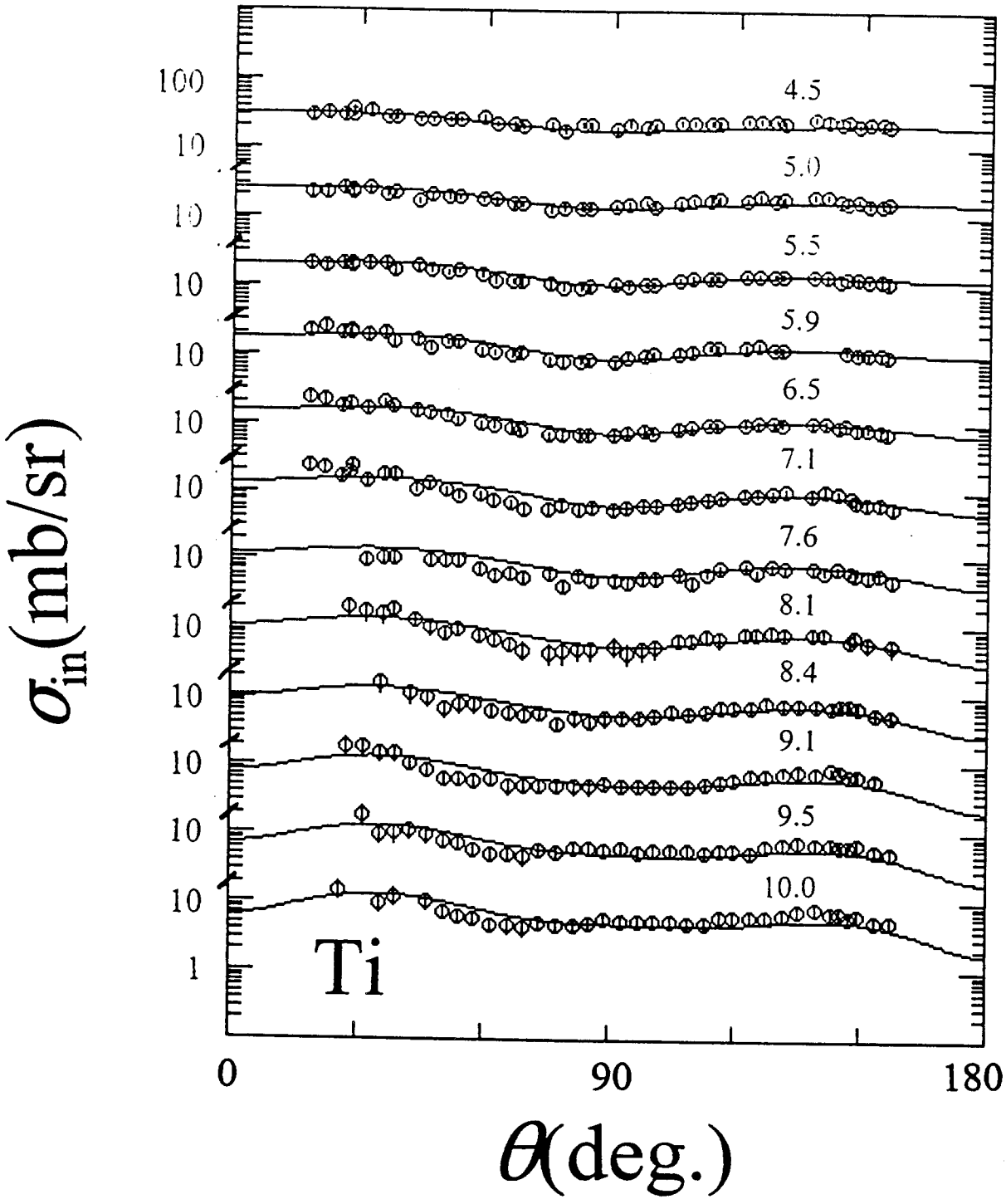

Fig. 4.4.4. Comparison of measured and calculated elemental cross sections for the excitation of the yrast 2^+ 984 keV level in ^{48}Ti. The experimental values are indicated by symbols and curves show the results of VIBM calculations. Incident neutron energies are numerically noted.

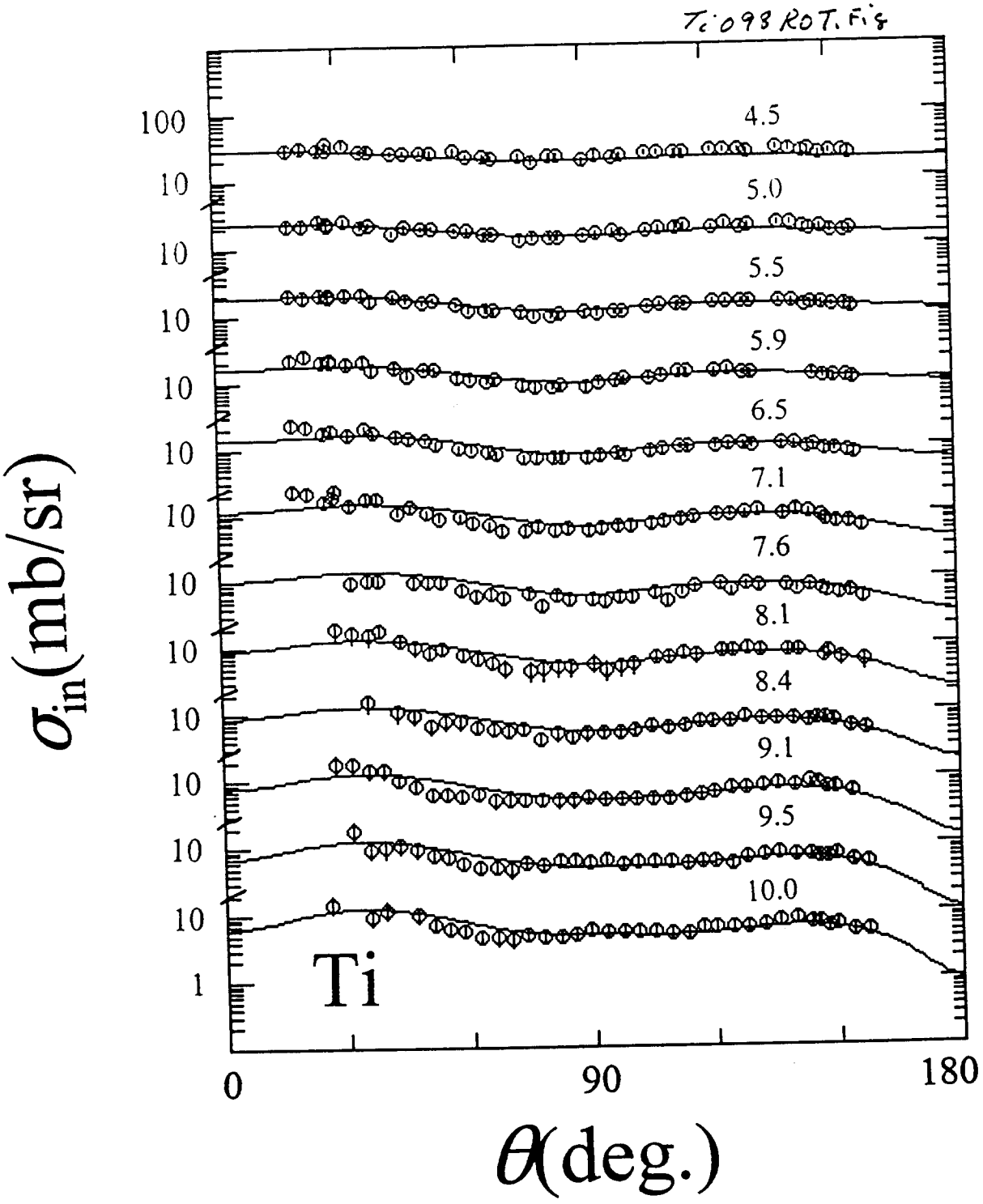

Fig. 4.4.5. Comparison of measured and calculated elemental cross sections for the excitation of the yrast 2+ 984 level in ^{48}Ti. The calculations employed the ROTM, otherwise the notation is identical to that of Fig. 4.4.4.

determined from six-parameter fitting and thus tend to scatter more than parameters determined with lesser degrees of freedom. This is particularly so for the spherical ISOM and ESOM potentials. Even given this scatter, the a_v of the spherical potentials agree to within ≈ 0.5% and are systematically smaller than the values for the VIBM and ROTM, which agree with one another to within ≈ 1.5%. None of the a_v were judged to have a significant energy dependence. The determination of r_v is complicated by the strong correlation with the real-potential depth. The fitting results below ≈ 1.5 MeV scattered rather badly, doubtless as a result of fluctuations, and were abandoned. The r_v of the ISOM and ESOM are quit similar and have significant energy dependencies. In contrast, the r_v of the collective models (VIBM or ROTM) have very weak (or no) energy dependencies. Here, as elsewhere in these remarks, parameter comparisons are made at 8 MeV. That energy is high enough to avoid the majority of the fluctuations evident at lower energy, is still well within the data base and the range of model validity, and is an energy where dispersion effects should not be large. The average of the four 8 MeV r_v is 1.2592 fm with an rms deviation from the mean of ≈ 1.1%. That is reasonable agreement that suggests that the spherical and collective r_v values are similar at 8 MeV though the former have a much stronger energy dependence and thus will not extrapolate well to higher energies. The determination of r_w values for all of the potentials was complicated by the presence of a broad dip in the r_w parameters resulting from the fitting in the ≈ 7.5 → 9.0 MeV region. This dip may be a consequence of residual fluctuation in the data. All the 14 MeV r_w values tended to lie quite high and were abandoned in determining r_w. These effects conspired to make the determination of r_w a somewhat subjective matter. As for the real potential, the r_w of the spherical models have a sharper energy dependence that those of the collective models. The average value of r_w at 8 MeV is 1.1719 fm, with an rms deviation from the mean of ≈ 2.5 %. Thus all of the 8 MeV r_w values are considerably less than the comparable r_v values. A similar tendency has been reported elsewhere in the region of the 3S maximum of the S_o strength function (e.g., Cr, Fe, Co and Ni). All of the a_w values become small as E → 0, and all of them tend to constant values at higher energies with the transition from energy dependence to constant values at lower energies for the collective potentials. The average 8 MeV a_w value is ≈ 0.6890 fm, ± ≈ 12%, which is a commonly encountered value.

The J_v of the spherical models have a much sharper energy dependence than those of the collective models. The magnitude of the slope is unusually large, and implies an unacceptably small reduced-mass ratio of $m^*/m \approx 0.1$ near the fermi surface [Bro+79]. Global spherical models typically have dJ_v/dE magnitudes of $\approx 2.8 \rightarrow 3.0$ fm^3 [BG69, WG86, Rap+79, Pat+76], and study of the equation of state over a very wide energy range gives a magnitude of ≈ 3.5 fm^3 [Bau+82]. All of these reported J_v slopes are approximately a third those of the present titanium SOMs, suggesting that the present spherical models are more a local parameterization of the neutron interaction with titanium than a global representation. Certainly, these spherical strengths can not reasonably be extrapolated beyond the energy range of the titanium data base. On the other hand, the collective J_v values have a rather weak energy dependence. The average of all four J_v values at 8 MeV is 457.8 MeV-fm^3, with an rms deviation from the mean of 1.5%. That is remarkably close agreement. The 8 MeV J_w values of the spherical models are in good agreement but approximately 30% larger than those of the collective models. Furthermore, they have a negative energy dependence while those of the collective models are approximately energy independent. Qualitatively, these behaviors are not surprising as the collective models take explicit account of the prominent low-lying inelastic channel. Moreover, the negative energy dependence of the J_w of spherical potentials in a collective environment is commonly observed. The consideration of volume absorption in the fitting procedures did not significantly improve the results. This is not surprising as the data base is at lower energies where volume absorption is not general believed to be significant.

The one-phonon vibrational models having β_2 values ranging from 0.01 to 0.30 gave essentially identical descriptions of the elastic-scattering data base, similar to that illustrated in Fig. 4.4.1. Total cross sections were also reasonably presented by models with $\beta_2 < 0.25$ (see Fig. 4.4.3 for an example). However, the inelastic-scattering cross section for the excitation of the yrast 2^+ level in ^{48}Ti at 984 keV was sensitive to the choice of β_2, as illustrated in Fig. 5.1. Values of $\beta_2 = 0.25$ certainly resulted in higher-energy inelastic-scattering cross sections, in the region where the direct reactions must be dominant, considerably larger than the observed values. A $\beta_2 = 0.15$ leads to calculated inelastic cross sections significantly lower than the present experimental results, and, to a lesser extent, lower than the measured values

of ref. [KP73]. Thus the interpretations suggest that β_2 is between 0.15 and 0.20, and probably nearer the latter value. Therefore, $\beta_2 = 0.20 \pm \approx 15\%$ was selected as the most realistic value. That $\beta_2 = 0.20$ of the VIBM is reasonably consistent with the results of coulomb-excitation and charged-particle studies, as discussed below. Calculations with this value give a very good description of the present inelastic-scattering results, a reasonable description of those of ref. [KP73] and an acceptable description of the lower energy results reported in the literature, given the fluctuations at lower energies (see Fig. 5.1). A good representation of the differential elastic scattering was achieved, as illustrated in Fig. 4.4.1, except at the very lowest energies (e.g., below ≈ 1 MeV) where there are very large partially-resolved resonance fluctuations in the measured data. From 3 → 8 MeV the VIBM total cross sections tend to be a bit larger than the experimental results, from 8 → 14 MeV the agreement is good, and then the calculated values are slightly lower on up to ≈ 25 MeV. The latter energy region is an extrapolation of the VIBM as there is no scattering data in this region upon which to base the model derivations (see remarks of Section 4). Below ≈ 3 MeV the VIBM total cross sections are consistently larger than the energy-average of the measured values. The discrepancy is well beyond what can be attributed to fluctuations, and it is not evident in the differential elastic-scattering cross-sections of Fig. 4.4.1. above ≈ 1.2 MeV. It is possible that the measurements in this fluctuating region were significantly distorted by self-shielding effects which could lead to anomalously small measured values. On the other hand, the inability of general and higher-energy potentials to fit the total cross section in the low-energy region in this mass region, despite reasonably strength functions, is well known. In the present ^{48}Ti case, all of the models of this work give S_o strength functions that are consistent with what is known from experimental measurements [MDH81], as shown in Table 4.3.3. The calculated S_1 values spread over a factor of approximately two, with collective models giving the larger values. There appear to be no experimental S_1 values for comparison. The VIBM reasonably represents the differential inelastic-scattering cross sections for the excitation of the yrast 2^+ level at 984 keV (see Fig.4.4.4). The magnitudes of the cross sections are consistent with the observations, as also indicated in Fig. 5.1, with the biggest differences between measured and calculated values at very forward and back angles at the highest measured energies. Experimental titanium polarization information is largely confined to the results of refs. [ZJ74 and FWW66]. However, it is encouraging that the VIBM model gives a satisfactory description of the observed values, as illustrated in Fig. 5.2. This suggests that the spin-orbit aspects of the VIBM potential are essentially correct. Generally, given the simplicity of the

one-phonon VIBM, the agreement with the neutron observables is quite satisfactory.

Systematics [Adl+56, SW55] and a number of charged-particle studies [Lut+69, Lut+74, Err67, SBD63, Per+70, Ber+68 and YS67] imply that a rotational model is not particularly appropriate for the neutron interaction with Ti. However, the ROTM was examined with results very similarly to those obtained with the VIBM. Again the differential elastic scattering was well described above ≈ 1 MeV, irrespective of the value of β_2 (see Fig. 4.4.2 as an example). The cross sections for the inelastic excitation of the yrast 2^+ 984 keV level in ^{48}Ti were best described with a ROTM having a $\beta_2 \approx 0.20$, as illustrated in Fig. 5.3, and this is reflected in the inelastic angular distributions shown in Fig. 4.4.5. Below ≈ 14 MeV, the ROTM total cross sections are similar to those obtained with the VIBM, as illustrated in Fig. 4.4.3. Above 14 MeV the ROTM total cross sections fall considerably below the measured values (and the VIBM results), but this discrepancy may not be significant as the model is being extrapolated well beyond the data base from which it was developed. Thus, comparisons of the ROTM and VIBM with the available experimental neutron data does not offer any clear guidance as to the reaction mechanism, although the above-cited evidence clearly suggests the vibrational reaction.

The above VIBM (and ROTM) is a very simple approximation, and the reality is probably far more complex. As a first step toward that increased complexity the vibrational potential derivation was repeated assuming a one- and two-phonon vibrational model with a $\beta_2 = 0.20$, following the fitting procedures described in Section 4 (herein this model is termed the 2PVIBM). A similar approach has been taken in studies of proton scattering from titanium; e.g., see ref. [Lut+69]. The yrast 2^+ level at 0.984 MeV was assumed to be the one-phonon state. The two-phonon triad was assumed to consist of the 4^+ 2.296 MeV, 2^+ 2.421 MeV and 0^+ 2.997 MeV levels. These four excited levels and the ground state were coupled assuming a β_2 of 0.20 thoughout. All other aspects of the calculations and fitting procedure were identical to those described in Section 4 for the VIBM. The resulting 2PVIBM potential parameters are given in Table 5.1. They are remarkably similar to those of the simple VIBM as given in Table 4.4.1. The description of the elastic scattering obtained with the 2PVIBM was essentially the same as that from the VIBM (compare Fig. 5.4 and Fig. 4.4.1). The 2PVIBM total cross sections were slightly larger than those of the VIBM, but probably insignificantly so. Cross sections for the excitation of the one-phonon state were approximately 20% lower than obtained with the VIBM, and thus somewhat lower than

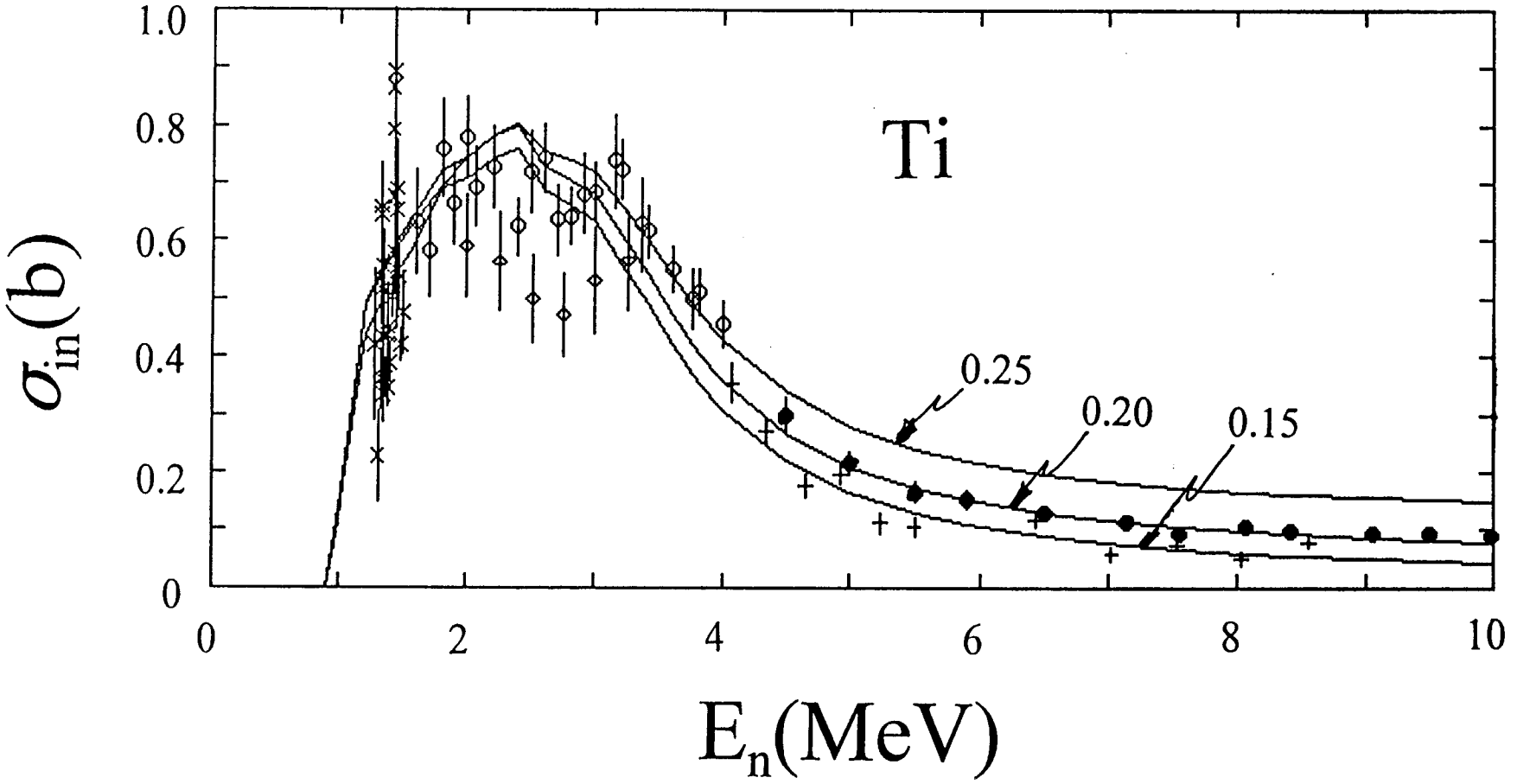

Fig. 5.1. Comparison of measured and calculated cross sections for the excitation of 984 keV level in elemental titanium. The solid circular symbols indicate the results of the present work, open circular symbols previous and lower-energy work from this laboratory [Smi+78], cross symbols the results of ref. [KP73], "X" symbols values from ref. [Bar+74], and diamond symbols from ref. [Ram75]. Curves indicate the results of VIBM calculations with the β_2 values numerically indicated.

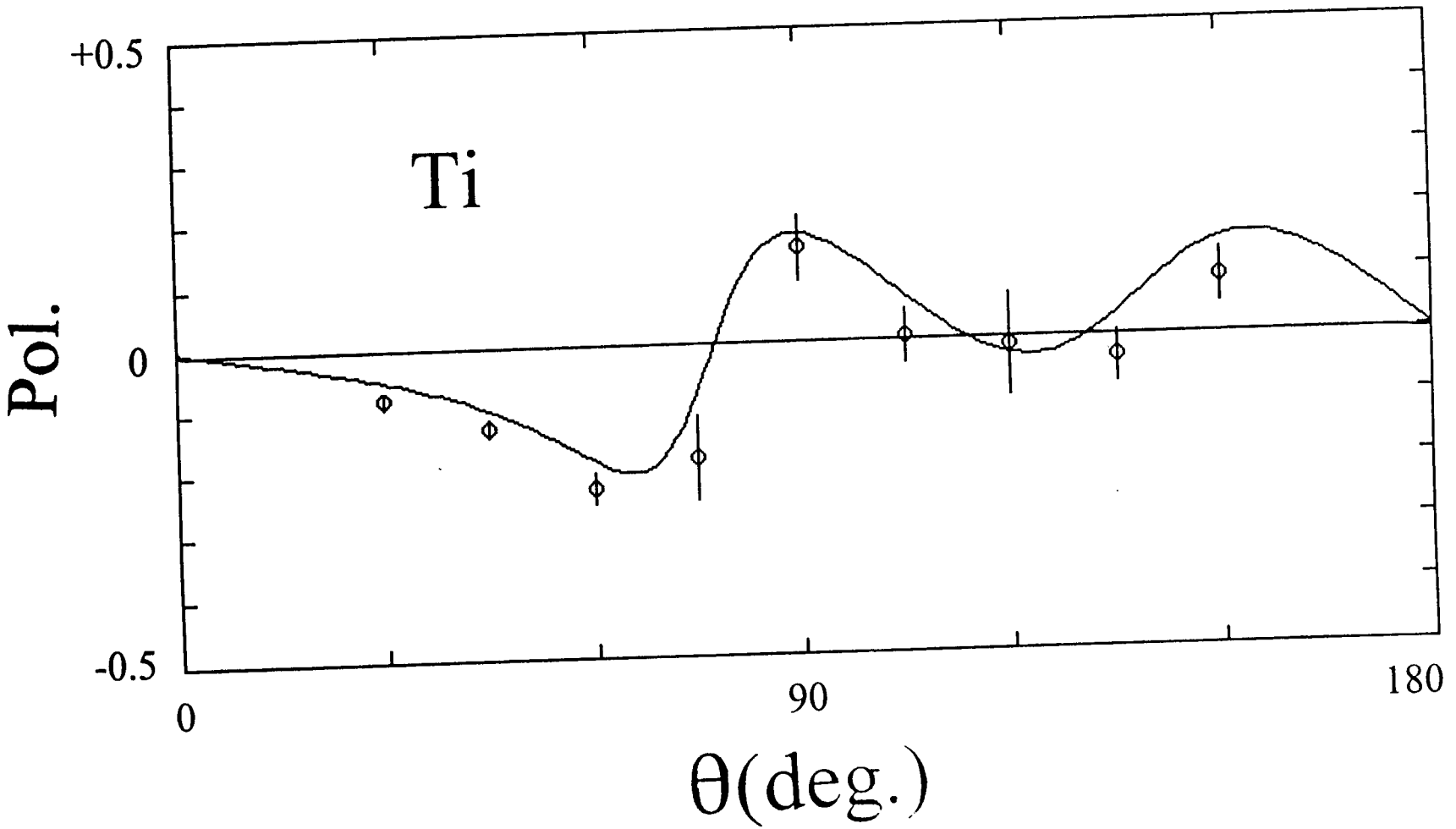

Fig. 5.2. Comparison of measured (symbols) and calculated (curve) polarization of 3.2 MeV neutrons scattered from elemental titanium. The experimental results are from ref. [ZJ74], and the calculations were obtained using the VIBM model with β_2 = 0.2.

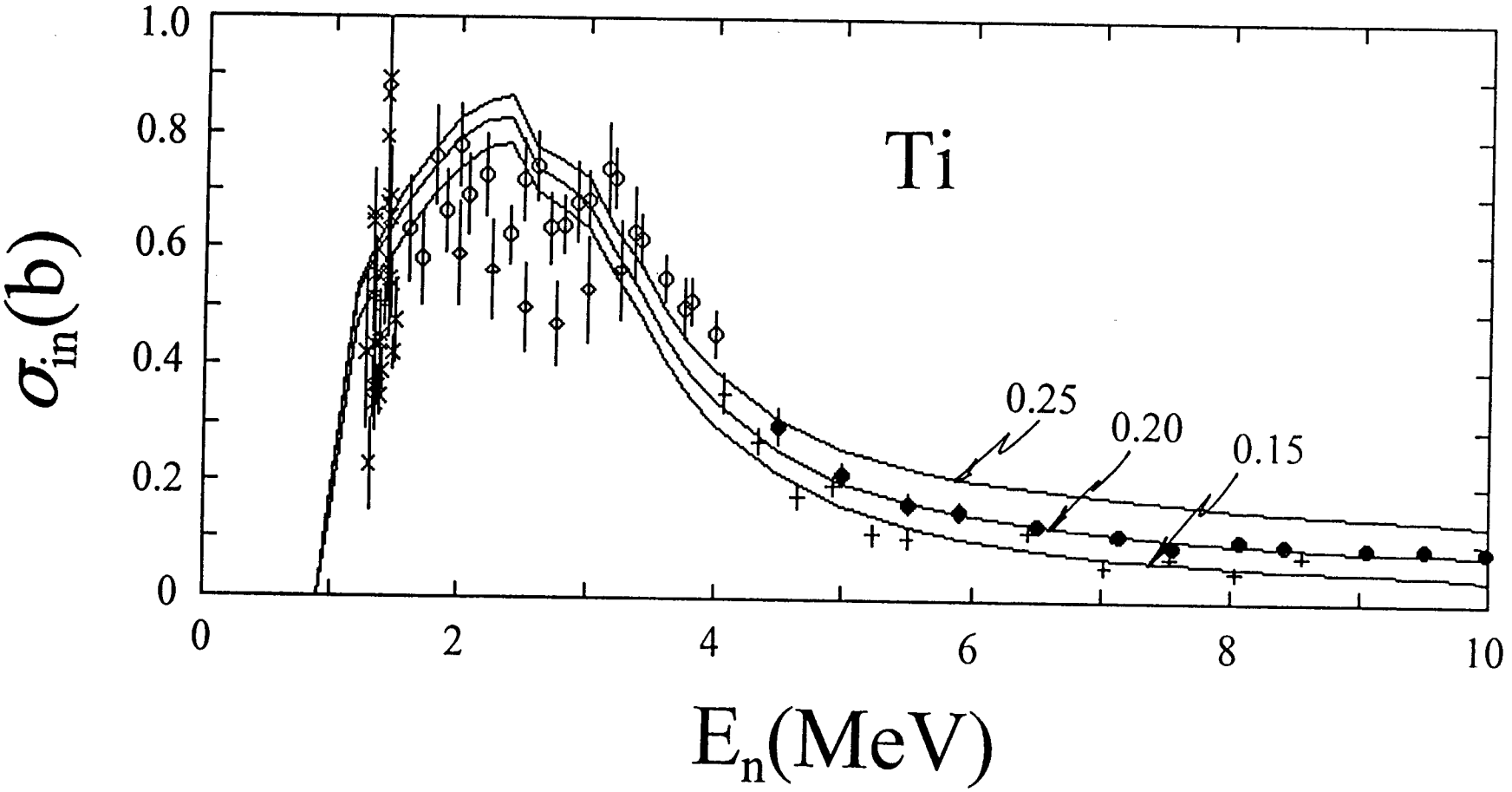

Fig. 5.3. Comparison of measured and calculated cross sections for the excitation of the 984 keV level in elemental titanium. The notation is identical to that of Fig. 5.1, except that the calculations were made with the ROTM.

the general trend of the experimental values as shown, for example, in Fig. 5.1. The experimental definition of the inelastic excitation of the two-phonon levels is not sufficient for meaningful experimental comparisons. If one increases β_2 to approximately 0.22 the 2PVIBM model will give inelastic-scattering results similar to those of the VIBM. Charged-particle work has suggested octupole vibrations in ^{48}Ti at excitations above ≈ 3 MeV (e.g., refs. [Lut+69] and [SBD63]). However, before one can justify the additional complexity of two-phonon and octupole levels the experimental neutron information must be considerably refined, particularly on an isotopic basis, with improved scattered-neutron resolution.

It has long been known that the real, V, and imaginary, W, potentials are correlated through the dispersion relationship [Sat83] given by

$$V(r,E) = V_{HF}(r,E) + \frac{P}{\pi}\int_{-\infty}^{+\infty}\frac{W(r,E')dE'}{(E-E')}, \qquad (5.1)$$

where V_{HF} is the Hartree-Fock potential and "P" denotes the principal value of the integral. This relationship influences the geometries and strengths of the potential and leads to the so-called "Fermi Surface Anomaly" at the lower energies typical of the present titanium study [JLM76]. The geometry dependence of Eq. 5.1 is mitigated when it is expressed in terms of volume-integrals-per-nucleon, J_i. In that form, Eq. 5.1 becomes

$$J_v(E) = J_{HF}(E) + \frac{P}{\pi}\int_{-\infty}^{+\infty}\frac{J_w(E')dE'}{(E-E')}. \qquad (5.2)$$

The integral can be broken into the surface, ΔJ_{ws}, and the volume, ΔJ_{wv}, components

$$\Delta J_{ws}(E) = \frac{P}{\pi}\int_{-\infty}^{+\infty}\frac{J_{ws}(E')dE'}{(E-E')}, \qquad (5.3)$$

$$\Delta J_{wv}(E) = \frac{P}{\pi}\int_{-\infty}^{+\infty}\frac{J_{wv}(E')dE'}{(E-E')}, \qquad (5.4)$$

and then

$$J_v(E) = J_{eff}(E) + \Delta J_{ws}(E), \qquad (5.5)$$

where $J_{eff}(E) = J_{HF}(E) + \Delta J_{wv}(E)$. $J_{HF}(E)$ and $\Delta J_{wv}(E)$ were

Table 5.1. Parameters for the 2PVIBM potential with β_2 = 0.20 and with one- and two-phonon vibrational excitations. The notation is identical to that of Table 4.3.1. There were four iterations of the initial parameters in the fitting procedure.

Real Potential

$J_v = 478.0 - 1.9464 \cdot E$ (462.4)

$r_v = 1.2734$ (1.2734)

$a_v = 0.6277$ (0.6277)

Imaginary Potential

$J_w = 52.7 + 0.3939 \cdot E$ (55.9)

$r_w = 1.2936 - 0.01201 \cdot E$ (1.1975)

$a_w = 0.321 + 0.06275 \cdot E \quad (E \leq 5)$ (0.6343)

$= 0.6343 \quad (E > 5)$

Spin-Orbit Potential (the same as Table 4.3.1)

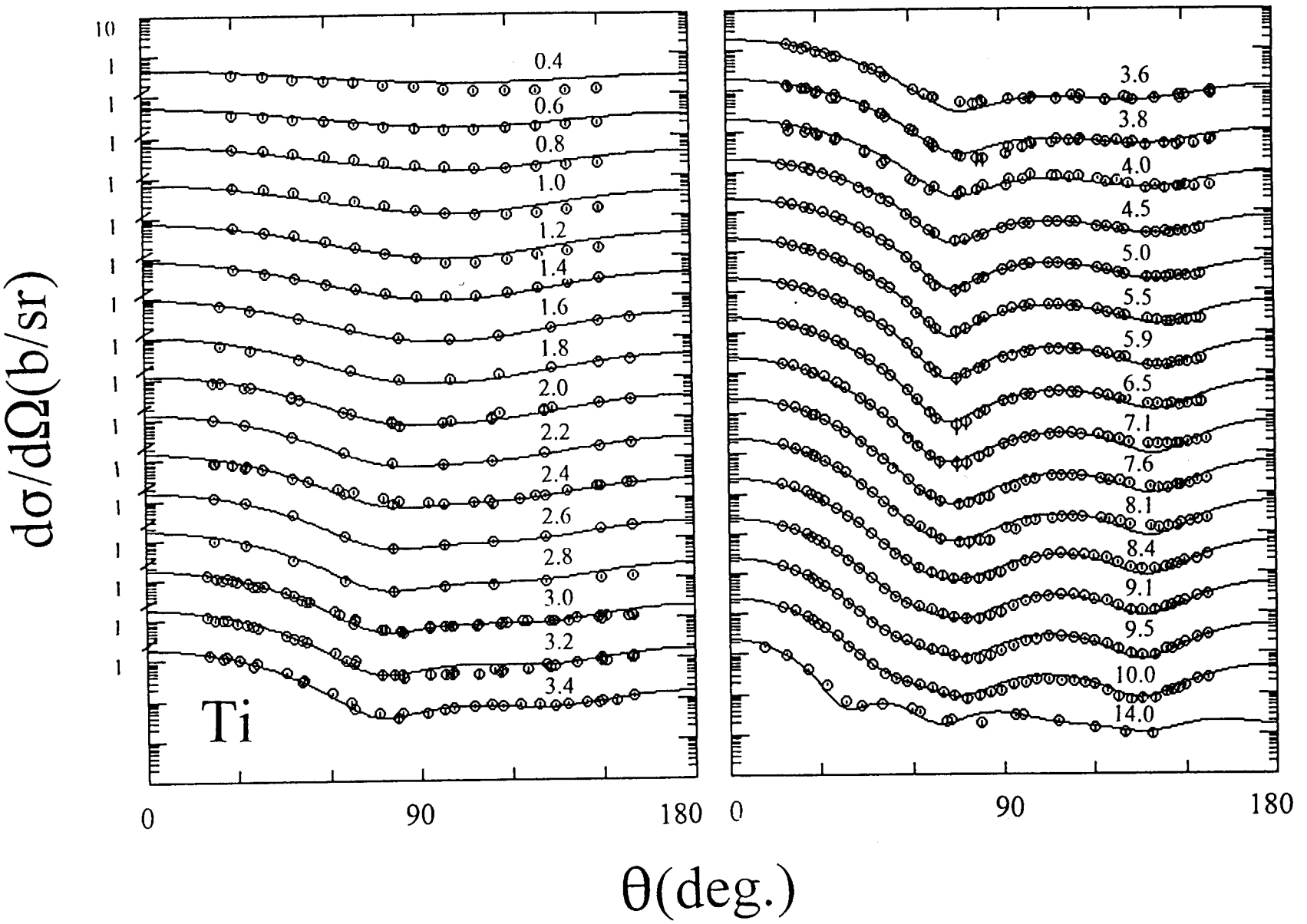

Fig. 5.4. Comparison of measured (symbols) and calculated (curves) differential elastic scattering cross sections. The calculations employed the 2PVIBM of the text. The notation is identical to that of Fig. 4.3.1.

assumed to have the same radial SW form factor, and $\Delta J_{ws}(E)$ the SW-derivative form factor. Within ≈ 25 MeV of the Fermi Energy, $\Delta J_{wv}(E)$ is essentially a linear function of energy, as is $J_{HF}(E)$, and not large irrespective of the details of the evaluation of Eq. 5.4. Thus the J_{HF} and ΔJ_{wv} components of J_{eff} are not experimentally separable. It is useful to define the ratio

$$\lambda(E) = \Delta J_{ws}(E)/J_{ws}(E), \qquad 5.6$$

where λ is the quantity by which J_{ws} is multiplied to obtain the surface-peaked component of the real potential, ΔJ_{ws}.

The above integrals were evaluated assuming the target consisted entirely of ^{48}Ti, and that the Fermi Energy, E_F, is -9.885 MeV as derived from the separation energies following from the mass tables. The imaginary potential was taken to be symmetric about the Fermi Energy as suggested by Mahaux and Sartor [MS86]. For energies $2 \cdot E_F < E < 0$, J_{ws} was assumed to have the form $J_{ws} = (J_o/E_F^2)(E-E_F)^2$, where J_o is the value of J_{ws} at $E \rightarrow 0$. For $0 < E < 20$ MeV, J_{ws} was taken from the VIBM of Table 4.4.1. Above 20 MeV the J_{ws} was assumed to linearly decrease with energy to a zero value at 60 MeV. Concurrently, J_{wv} rises from zero at 20 MeV to a value of 50 MeV-fm^3 at 60 MeV and remains constant to higher energies. This is a simple linear-segment model. The experimental evidence does not justify a more complex representation (e.g., as given in refs.[DF90] or [MS86]) in the case of neutron scattering from titanium. In the energy region of the present considerations, the resulting ΔJ_{ws} and ΔJ_{wv} are not particularly sensitive to the exact choice of the parameterizations. The "λ" of Eq. 5.6 rises monotonically from negligible values at E ≈ 14 MeV to approximately 0.5 as the energy decreases towards zero.

With the above assumptions, the "λ" of Eq. 5.6 was calculated and used to add a Saxon-Woods-derivative surface component to the Saxon-Woods real potential which in turn was used to repeat the entire fitting procedure of the VIBM, outlined above. As for the VIBM, a vibrational one-phonon coupling model with $\beta_2 = 0.20$ was assumed. The output was used to re-evaluate "λ" and the fitting repeated through two iterations. The parameters of this new potential, termed the "DVIBM", are given in Table 5.2. The DVIBM gives essentially the same description of the elastic-scattering data as the VIBM (compare Figs. 4.4.1 and 5.5). The calculated total and inelastic-scattering cross sections and the strength functions (see Table 4.3.3) are also

very similar. The main difference between VIBM and DVIBM models is in the real-potential strength where that of the DVIBM is less than that of the VIBM. That effect is expected as the former does not include the ΔJ_{ws} contribution that has been specifically treated in the DVIBM calculations. Since $\Delta J_{wv} \approx 5.0 + 0.5 \cdot E$ over the energy range of the present experiments, J_{HF} must be approximately $J_{HF} = 455.0 - 1.4 \cdot E$ MeV-fm^3. The fact that J_{HF} is energy dependent reflects the non-locality of the interaction and the finite nuclear size. It is this J_{HF} that should be used in the global comparisons as, at least in a first approximation, the effects of structure have been removed.

It is well known that dispersive effects are most pronounced in the bound region. There are only four bound particle states in ^{48}Ti between zero energy and the fermi energy ($2p_{1/2}$, $2p_{3/2}$, $1f_{5/2}$, $1f_{7/2}$). This is a region where an extrapolation of the present neutron potentials to the bound states should be reasonably reliable and where there should be sensitivity to dispersive effects. All the bound hole states lie much deeper ($<\approx -20$ MeV) and thus beyond a reasonable extrapolation of the present potentials. The binding energies of the above four particle states follow from the systematics of Millener and Hodgson [MH73], which are based upon experimental stripping and pickup studies. The DVIBM and VIBM potentials were extrapolated into the bound region and used to calculate the binding energies (BE) of the above four particle states assuming a simple SW potential form. The resulting calculated binding energies are compared with those based upon measurements in Table 5.3. The average deviation of the DVIBM BE values from the experimental quantities is $\approx$ 0.54 MeV, and that of the VIBM $\approx$ 0.73 MeV. Thus the DVIBM tends to be somewhat more descriptive of the experimental particle BEs.

The author and his co-workers have reported a number of studies of fast-neutron scattering from which SOM potentials were derived. They range from A = 40 and a nuclear asymmetry of 0 to A = 238 and an asymmetry of 0.227 [Smi94, SG93, LGS89, SS97, Smi96, Smi+88, LGS87, SC96, SGL88, Smi+92A, LGS86, Chi+92, SGL86, SG94A, SG94B, Smi97, SG94, Chi+90, Smi95]. These results, combined with the present titanium study, provide twenty potentials for determining the systematic trends of the SOM with target mass and nuclear asymmetry. Many of the potential parameters are energy dependent and all of them are based upon neutron data at energies of $<\approx$ 20 MeV where dispersive effects may be present. It was suggested in refs. [Chi+90] and [LGS90] that comparisons at $\approx$ 8 MeV are rewarding as the energy is high enough so that fluctuation distortions are minimized, dispersive

Table 5.2. Parameters for the DVIBM potential with $\beta_2 = 0.20$ and including contributions from the dispersion integral. The notation is identical to that of Table 4.3.1. There were four iterations of the initial parameters in the fitting procedure.

Real Potential

$J_v = 460.0 - 0.9304 \cdot E$ (452.5)

$r_v = 1.2710 - 0.001198 \cdot E$ (1.2614)

$a_v = 0.6252$ (0.6252)

Imaginary Potential

$J_w = 52.6 - 0.1922 \cdot E$ (51.1)

$r_w = 1.3194 - 0.02286 \cdot E$ (1.1365)

$a_w = 0.361 + 0.04484 \cdot E \quad (E \leq 8)$ (0.7197)

$= 0.7194 \quad (E > 8)$

Spin-Orbit Potential (the same as Table 4.3.1)

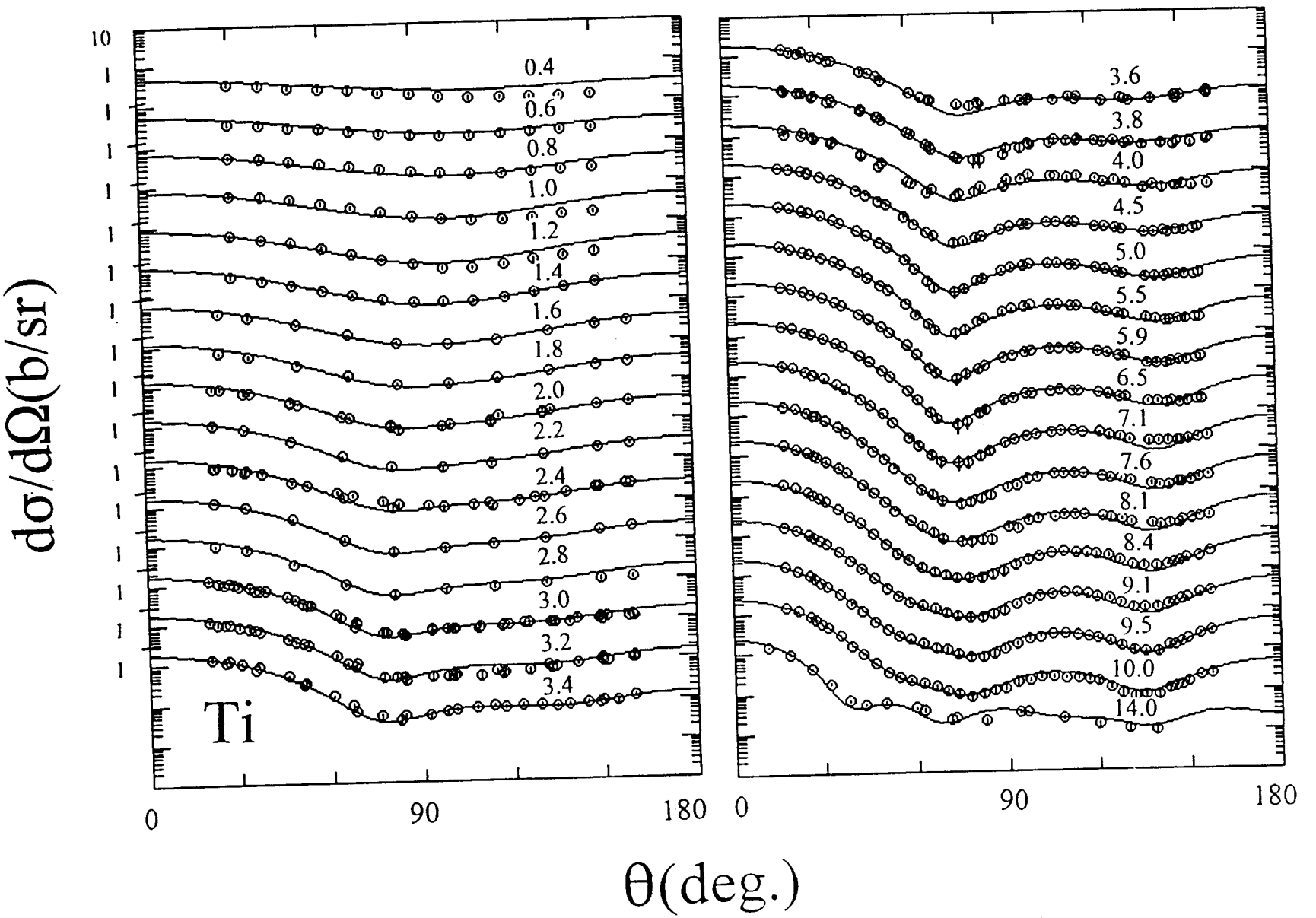

Fig. 5.5. Comparisons of measured (symbols) and calculated (curves) differential elastic scattering cross sections of elemental titanium. The calculations employed the DVIBM of the text. The notation is identical to that of Fig. 4.3.1.

Table 5.3. Measured and calculated binding energies of bound particle states in ^{48}Ti in MeV.

State	Exp.-BE [MH73]	DVIBM-BE	VIBM-BE
$2p_{1/2}$	4.312	4.542	3.489
$2p_{3/2}$	6.280	5.587	5.001
$1f_{5/2}$	3.050	3.881	2.250
$1f_{7/2}$	9.000	8.586	9.006

contributions are generally not large, and the energy is low enough to avoid uncertainties due to volume absorption. The a_v are generally energy independent with an average 8 MeV value for the twenty SOM potentials of 0.6495 ± 0.0411 fm (where the uncertainty is the rms deviation from the average). The present titanium a_v value is slightly smaller than this average and its associated uncertainty. The r_v of seventeen of these potentials (Pd, Rh and Cd values were neglected as anomalous) are reasonably consistent at 8 MeV, and well represented by the expression

$$r_v = 1.1685 + 0.37225/A^{1/3}, \qquad (5.7)$$

where A is the target mass. The rms deviation of the individual r_v values from the systematic trend of Eq. 5.7 is ≈ 0.8%, and present titanium value is very consistent with this uncertainty. The constants of Eq. 5.7 are quite similar to those of ref. [Chi+90], which were based on a much more limited data base, and the expression is similar to the model Moldauer [Mol63] proposed many years ago. They are also similar to those deduced by Meyers from proton-reaction considerations [Mey73]. The real-potential strengths, J_v, are related to the nuclear asymmetry $\eta \equiv (N-Z)/A$ by

$$J_v = J_o(1 \pm \xi \cdot \eta), \qquad (5.8)$$

where J_o and ξ are constants and "-" ("+") refers to neutrons (protons) [Lan62]. Fitting Eq. 5.8 to the J_v of the twenty SOMs leads to a J_o = 489.1 MeV-fm^3 and ξ = 0.969. These values are similar to the 480 MeV-fm^3 and 0.98 of ref. [HW72], the 495±30 MeV-fm^3 and 0.95 of Ferrer et al. [FCR77], and the 486.8 MeV-fm^3 and 1.04 of ref. [Chi+90]. All of these ξ values are approximately a factor of two larger than suggested by nucleon-nucleon scattering and (p,n) studies. However, these simple ξ results, derived from a mass distribution of potentials, are distorted by approximately a factor of two due to the size effect. More accurately, Eq. 5.8 should take the form [Chi+90]

$$J_v = r_v^3 K_o(1 \pm \xi \cdot \eta), \qquad (5.9)$$

where K_o is a constant and r_v has the form of Eq. (5.7). Fitting Eq. 5.9 to the J_v values of the above twenty potentials gives K_o = 233.2 MeV-fm^3 and ξ = 0.496. The latter ξ is similar to the 0.53 value of ref. [Chi+90], the 0.48 suggested by nucleon-nucleon scattering [GMP70, GPT68], and the 0.4 indicated

by (p,n) studies [BFG69]. The size effect on ξ has frequently been ignored in the literature. The above indicates that the real portion of the SOM follows a systematic behavior with mass and asymmetry as set forth in Eqs. 5.7 and 5.9, and these trends are consistent with the present titanium SOM. Similar trends of the imaginary portion of the SOM are not as clear as that potential reflects the structure of the individual targets and thus the parameters tend to scatter by rather large amounts that make systematic comparisons difficult. The above systematic behaviors are influenced by dispersion effects that are not widely or well enough known for inclusion in the considerations. Collective interactions are also a factor but they tend to be specific to the particular nuclei and thus not consistent with systematic trends.

There have been a number of studies of proton scattering from ^{48}Ti reported in the literature from which conventional spherical optical models have been deduced. Perey and Perey [PP76] cite thirteen such studies at energies of ≈ 6 to 25 MeV. Of these, nine of the resulting potentials are relatively consistent and were used for comparison with the present neutron ESOM results. The proton and neutron potentials are related through the asymmetry relationship of Eq. 5.8. To carry out the comparisons the reported proton real-potential depths were corrected for the coulomb effect using the well known expression $V_c = 0.4 \cdot Z/A^{1/3}$. Then the proton potential depths were adjusted for the asymmetry effect assuming an isovector potential of 20 MeV (see Eq. 5.8). The result is not very sensitive to the latter choice as the asymmetry is small in the present ^{48}Ti case. With these adjustments, the proton potentials imply a neutron potential having a real strength given by $J_v = 474.5 - 4.679 \cdot E$. Both the $E \rightarrow 0$ intercept and the energy dependence of this strength are considerably less than those of the ESOM. However, in an energy region of reasonable overlap the strengths are similar. For example, at 8 MeV the quantity $(J_v(\text{ESOM}) - J_v(p,p))/J_v(\text{ESOM})$ equals +4.1%, at 10 MeV = +2.2% and at 14 MeV = -2.3%. The present ESOM should not be extrapolated to higher energies, and the lower energy behavior of the proton potentials is obscured by coulomb effects.

Comparisons of β_2 values are meaningful in the context of the deformation length $\delta_2 = R_v \cdot \beta_2$ (where $R_v = r_v \cdot A^{1/3}$) [Bla63]. The electromagnetic (em) β_2 values for the even-even titanium isotopes rapidly decrease with mass from 0.316 at ^{46}Ti, to 0.166 at ^{50}Ti, with the ^{48}Ti value of 0.269 [Ram+87]. This behavior is consistent with a linear dependence of β_2 on nuclear asymmetry (η) given by $\beta_2 = 0.411(1 - 4.75 \cdot \eta)$. In the present neutron

study it was assumed that the β_2^{nn} values were entirely attributable to ^{48}Ti, therefore the β_2^{nn} should be compared with β_2^{em} of ^{48}Ti. The em values were deduced assuming r_v^{em} = 1.2 fm [Ram+87], thus δ_2^{em} = 1.173 fm for ^{48}Ti. The corresponding neutron value following from the VIBM is δ_2^{nn} = 0.924 (±10%) fm. Corresponding values of δ_2^{pp} result from (p,p') studies reported in the literature (e. g., [Lut+69, Lut+74, Per+70, Err67]). They scatter by large amounts, ranging from ≈ 0.82 to ≈ 1.2 fm. Clearly, $\delta_2^{nn} < \delta_2^{em}$. This is qualitatively consistent with the predictions of the core-polarization model of Madsen, Brown and Anderson [MBA75] and ref. [BM75], assuming the target is a proton vibrator with the closed neutron shell. Such a model is explicitly relevant to ^{50}Ti, and the model assumptions may be approached in the ^{48}Ti case as the $f_{7/2}$ shell is only two neutrons short of closure. Concurrently, this version of the model predicts that $\delta_2^{pp} < \delta_2^{nn}$. Unfortunately, due to the scatter of δ_2^{pp} values, the latter inequality can not be verified. The core-polarization model is strictly applicable to single-closed shell nuclei. Off closed shells both neutrons and protons may well be excited thus the predictions of the model in the present case are probably limiting values.

The present neutron deformation can also be compared with electro magnetic properties using the normalized moments method of Hamilton and Mackintosh [HM78], the VIBM potential of Table 4.4.1, and the the electro magnetic results deduced from coulomb-excitations as complied in ref. [Ram+87]. The quadrupole moment of the real vibrational field, q_{20}, is given by

$$q_{20} = \int_o^\infty r^4 \, \mathrm{Re}\, F_2(r)\, dr \qquad (5.10)$$

where

$$\mathrm{Re}\, F_2(r) = \beta_2 \, (d/dr) \, [R \cdot V(r)], \qquad (5.11)$$

R is the real Saxon-Woods potential radius ($R = r_o \cdot A^{1/3}$), and V(r) is the Saxon-Woods real potential. This moment is normalized to the volume integral of the potential,

$$J = 4\pi \int_0^\infty r^2 \cdot V(r)\, dr, \qquad (5.12)$$

to obtain a "normalized moment", Q_{20}, given by

$$Q_{20} = q_{20}/J. \qquad (5.13)$$

B(E2) values follow from

$$B(E2) = (ZQ_{20})^2 e^2. \qquad (5.14)$$

The VIBM potential leads to $B(E2)^{1/2} = 26.22$ $(e \cdot fm^2)$ for ^{48}Ti while the equivalent coulomb-excitation value from ref. [Ram+87] is 26.83 $(e \cdot fm^2)$. The agreement is certainly fortuitously good. Indeed, the results from the neutron potential perhaps should be somewhat the larger as they reflect the nuclear density distribution rather that the charge distribution alone. However, the comparison does support the validity of the β_2 of the present VIBM model.

Acknowledgments

The author is very much indebted to Dr. J. Raynal for assistance in a number of aspects of the coupled-channels calculations, to Dr. R. Haight and his associates for making available preliminary neutron total cross section data filling a void in the experimental data base, to Dr. P. E. Hodgson for helpful suggestions, and to the staff of the National Nuclear Data Center for providing a wide range of experimental numerical data.

References

[Adl+56] K. Adler, A. Bohr, T. Huus, B. Mottleson and A. Winther, Rev. Mod. Phys. 28 432 (1956).

[Bar+74] E. Barnard, J. deVilliers, P. Moldauer, D. Reitmann, A. Smith and J. Whalen, Nucl. Phys. A229 189 (1974); also Argonne National Laboratory Report, ANL/NDM-3 (1973).

[Bau+82] M. Bauer, E. Hermandez-Saldena, P. E. Hodgson and J. Quintanilla, J. Phys. G8 525 (1982).

[Ber+68] A. U. Berstein, E. P. Lippincott, G. T. Sample and C. B. Thorn, Nucl. Phys. A115 79 (1968).

[BBN62] C. Bowman, E. Bilpuch and H. Newson, Ann. Phys. 17 319 (1962).

[BFG69] C. J. Batty, E. Friedman and G. W. Greenlees, Nucl. Phys. A127 368 (1969).

[Bla63] J. S. Blair Direct interactions and nuclear reaction mechanisms p. 666 (Gordon and Breach, New York, 1963).

[BM75] V. R. Brown and V. A. Madsen, Phys. Rev. C11 1298 (1975).

[BG69] F. D. Becchetti Jr. and G. W. Greenlees, Phys. Rev. 182 1190 (1969).

[Bro+79] G. E. Brown, J. S. Dehesa and J. Speth, Nucl. Phys. A330 290 (1979).

[CGB52] J. Coon, E. Graves and H. Barschall, Phys. Rev. 88 56 (1952).

[Chi+90] S. Chiba, P. T. Guenther, R. D. Lawson and A. B. Smith Phys. Rev. C42 2487 (1990).

[Chi+92] S. Chiba, P. T. Guenther, A. B. Smith, M. Sugimoto and R. D. Lawson, Phys. Rev. C45 1260 (1992).

[CL55] L. Cranberg and J. Levin, Proc. Conf. on Peaceful Uses of Atomic Energy, Geneva (United Nations Press, New York, 1955).

[CSL83] Nuclear Standards File, IAEA Tech. Report 227, eds. H. Conde, A. Smith and A. Lorenz (1983).

[CW55] V. Culler and R. Waniex, Phys. Rev. 99 740 (1955).

[DF90] R. K. Das and R. W. Finlay, Phys. Rev. C42 1013 (1990).

[Dju72] A. Djumin, Izv. Akad. Nauk SSSR, Ser. Fiz 36 852 (1972).

[Dro87] M. Drosg, IAEA Report, IAEA-TECDOC-410 (1987).

[Err67] H. J. Erramuspe, Nucl. Phys. A101 138 (1967).

[FCR77] J. C. Ferrer, J. D. Carlson and J. Rapaport, Nucl. Phys. A275 325 (1977).

[FG71] D. Foster and D. Glasgow, Phys. Rev. C3 576 (1971).

[FWW66] A. T. G. Ferguson, R. W. White and D. Wetmore, Nucl. Phys. 66 369 (1966).

[GC65] A. Gilbert and A. Cameron, Can. J. Phys. 43 1446 (1965).

[GMP70] G. W. Greeenlees, W. Makafshe and G. J. Pyle, Phys. Rev. C1 1145 (1970).

[Goo52] L. Goodman, Phys. Rev. 88 686 (1952).

[Goo+66] W. Good, D. Paya, R. Wagner and T. Tamura, Phys. Rev. 151 912 (1966).

[GPT68] G. W. Greeenlees, G. J. Pyle and Y. C. Tang, Phys. Rev. 171 1115 (1968).

[Gue+78] P. Guenther, D. Havel, A. Smith and J. Whalen, Argonne National Laboratory Report, ANL/NDM-31 (1977).
[GRH71] J. Garg, J. Rainwater and W. W. Havens Jr., Phys. Rev. C3 2447 (1971).
[Hai+96] R. Haight et al., private communication (1996).
[HF52] W. Hauser and H. Feshbach, Phys. Rev. 87 362 (1952).
[HM78] J. K. Hamilton and R. S. Mackintosh, J. Phys. G4 557 (1978).
[Hod71] P. E. Hodgson, Nuclear reactions and nuclear structure (Clarendon, Oxford, 1971).
[HW72] B. Holmqvist and T. Wiedling, Nucl. Phys. A188 24 (1972).
[KP73] W. E. Kinney and F. G. Perey, Oak Ridge National Laboratory Report, ORNL-4810 (1973).
[JLM76] J. P. Jeukenne, A. Lejeune and C. Mahaux, Phys. Reports C25 83 (1976).
[Lan62] A. M. Lane, Nucl. Phys. 35 676 (1962).
[Las51] A. Lasday, Phys. Rev. 81 139 (1951).
[Law80] R. D. Lawson, Theory of the nuclear shell model (Clarendon, Oxford, 1980).
[LGS86] R. D. Lawson, P. T. Guenther and A. B. Smith, Phys. Rev. C34 1559 (1986).
[LGS87] R. D. Lawson, P. T. Guenther and A. B. Smith, Phys. Rev. C36 1298 (1987).
[LGS89] R. D. Lawson, P. T. Guenther and A. B. Smith, Nucl. Phys. A493 267 (1989).
[LGS90] R. D. Lawson, P. T. Guenther and A. B. Smith, Nucl. Phys. A519 587 (1990).
[Lut+69] H. F. Lutz, W. Bartolini, T. H. Curtis and G. H. Klody, Phys. Rev. 87 1479 (1969).
[Lut+74] H. F. Lutz, D. W. Heikkinen, W. Bartolini and D. Proctor, Nucl. Phys. A231 365 (1974).
[MBA75] V. A. Madsen, V. R. Brown and J. D. Anderson, Phys. Rev. C12 1205 (1975); also Phys. Rev. C11 1298 (1975).
[Mey73] W. D. Meyers, Nucl. Phys. A204 465 (1973).
[MDH81] S. F. Mughabghab, M. Divadeenamn and N. E. Holden, Neutron cross sections (Academic, New York, 1981).
[MH73] D. J. Millener and P. E. Hodgson, Nucl. Phys. A209 59 (1973).
[Mol63] P. A. Moldauer, Nucl. Phys. 47 65 (1963).
[Mol80] P. A. Moldauer, Nucl. Phys. A344 185 (1980).
[Mol82] P. A. Moldauer, Spherical optical-model code ABAREX, private communication (1982); modified for elemental use by S. Chiba.
[MS86] C. Mahaux and R. Sartor, Nucl. Phys. A458 14 (1986).
[NDS] L. K. Peker, Nucl. Data Sheets 68 271 (1993); T. W. Burrows, Nucl. Data Sheets 74 1 (1995); T. W. Burrows, Nucl. Data Sheets 68 1 (1993); T. W. Burrows, Nucl. Data Sheets 48 569 (1986); T. W. Burrows, Nucl. Data Sheets 75 1 (1995).
[Pat+76] D. M. Patterson, R. R. Doering and A. Galonsky, Nucl. Phys. A263 261 (1976).
[Per+70] C. M. Perey, R. J. Silva, J. K. Dickens and F. G. Perey, Phys. Rev. C2 468 (1970).

[PP76] C. M. Perey and F. G. Perey, At. Data and Nucl. Data Tables 17 1 (1976).
[Ram75] E. Ramstrom, Studsvik Report, AE-503 (1975).
[Ram+87] S. Raman, C. H. Malarkey, W. T. Miller, C. W. Nestor Jr. and P. H. Stelson, At. Data and Nucl. Data Tables 36 1 (1987).
[Rap+79] J. Rapaport, V. Kulkarni and R. W. Finlay, Nucl. Phys. A330 15 (1979).
[Ray96] J. Raynal, The coupled-channels code, ECIS96, private communication (1996); also see the CEA Report, CEA-N-2772 (1994).
[Sat83] G. R. Satchler, Direct nuclear reactions (Clarendon, Oxford, 1983).
[SBD63] G. R. Satchler, R. N. Bassel and R. M. Drisko, Phy. Lett. 5 256 (1963).
[SC96] A. B. Smith and S. Chiba, Ann. Nucl. Energy 23 459 (1966).
[SGL86] A. B. Smith, P. T. Guenther and R. D. Lawson, Nucl. Phys. A455 344 (1986).
[SGL88] A. B. Smith, P. T. Guenther and R. D. Lawson, Nucl. Phys. A483 50 (1988).
[SGS77] A. Smith, P. Guenther and R. Sjoblum, Nucl. Instr. and Methods 140 397 (1977).
[SG93] A. B. Smith and P. T. Guenther, J. Phys. G19 655 (1993).
[SG94] A. B. Smith and P. T. Guenther, Nucl. Phys. A568 221 (1994).
[SG94A] A. B. Smith and P. T. Guenther, J. Phys. G20 795 (1994).
[SG94B] A. B. Smith and P. T. Guenther, Ann. Nucl. Energy 21 629 (1994).
[Smi+78] A. B. Smith, P. T. Guenther, P. A. Moldauer, J. F. Whalen, Nucl. Phys. A304 224 (1978).
[Smi+88] A. B. Smith, P. T. Guenther and R. D. Lawson, Nucl. Phys. A483 50 (1988).
[Smi91] A. B. Smith, Argonne National Laboratory memorandum (1991), unpublished.
[Smi+92] A. B. Smith and P. T. Guenther, Argonne National Laboratory Report, ANL/NDM-127 (1992); S. Chiba, P. Guenther, A. Smith, M. Sugimoto and R. Lawson, Phys. Rev. C45 1260 (1992); C. Budtz-Jorgensen, P. Guenther, A. Smith and J. Whalen, Z. Phys. A306 265 (1982); A. Smith, P. Guenther, R. Larsen, C. Nelson, P. Walker and J. Whalen, Nucl. Instr. and Methods 50 277 (1977); and references cited therein.
[Smi+92A] A. B. Smith, P. T. Guenther, J. F. Whalen and S. Chiba, J. Phys. G18 629 (1992).
[Smi94] A. B. Smith, Nucl. Phys. A576 165 (1994).
[Smi95] A. B. Smith, Nucl. Phys. A589 201 (1995).
[Smi96] A. B. Smith, Nucl. Phys. A605 269 (1996).
[Smi97] A. B. Smith, accepted for publication in Nucl. Phys.

[SML59] C. St. Peirre, M. Mackwe and P. Lorraine, Phys. Rev. 115 999 (1959).
[SS97] A. B. Smith and D. Schmidt, J. Phys. G23 197 (1997).
[SSH74] R. Schwartz, R. Schrack and H. Heaton, National Bureau of Standards Report, NBS-138 (1974).
[SW55] G. Scharff-Goldhaber and J. Weneser, Phys. Rev. 98 212 (1955).
[Tam65] T. Tamura, Rev. Mod. Phys. 17 679 (1965).
[WG86] R. L. Walter and P. P. Guss, Proc. Conf. on Nucl. Data for Basic and Applied Science, eds. P. Young et al. (Gordon and Breach, New York, 12986) p. 1079, vol. 2.
[YS67] J. L. Yntema and G. R. Satchler, Phys. Rev. 161 1137 (1967).
[ZJ74] E. Zijp and C. C. Jonker, Nucl. Phys. A222 93 (1974).